NATIONAL AND KAPODISTRIAN UNIVERSITY OF ATHENS

SCHOOL OF SCIENCE
DEPARTMENT OF INFORMATICS AND TELECOMMUNICATION

MSc THESIS

Angle-of-Arrival Measurement Techniques for Enhanced Positioning in Beyond 5G Systems

Ameen A Alfiza

Supervisor (or supervisors): **Nikos Passas,** Dr.

ATHENS

September 2021

MSc THESIS

Angle-of-Arrival Measurement Techniques for Enhanced Positioning in Beyond 5G Systems

Ameen A Alfiza

S.N.: SN1200018

SUPERVISOR: **Nikos Passas,** Dr**.**

ABSTRACT

The new generation of mobile communication systems introduces new methods and technologies that may enhance positioning accuracy in some scenarios when the GNSS system cannot meet the requirements, such as indoor positioning and outdoor autonomous driving. The 3GPP standard and for the first time included the angle measurement as new positioning methods in 5G. The Angle of Arrival (AoA) is the angle measurement method on the uplink direction that can enjoy the new capabilities in 5G systems to enhance the positioning downs to centimeters.

Multiple Signal Classification Method (MUSIC) is a high-accuracy super-resolution algorithm for AoA estimation. The MUSIC method for estimating AoA has many shortcomings that make it unsuitable for a wide variety of scenarios. Correlated multipath signals substantially reduce estimation accuracy. Additionally, this method is a searching algorithm that requires a significant amount of time to resolve AoA. In this thesis, a CASCADE algorithm was proposed to overcome MUSIC's constraints by estimating a coarse range of AoA using a rapid AoA algorithm and then passing that range to the second stage represented by MUSIC to estimate AoA correctly. Multipath signals were eliminated by modifying the proposed CASCADE to detect only the line of sight (LOS), which is the essential path for angular localization.

Additionally, the thesis compares many AoA algorithms in the context of 5G systems. A sounding reference signal (SRS) in the mm-wave band was generated according to the 3GPP standards and utilized as the input to those algorithms.

A simulation was conducted throughout this thesis by evaluating six AoA algorithms: Bartlet Beamforming, MVDR, MUSIC, ESPRIT, FFT, and the proposed CASCADE method. The results showed that the proposed algorithm achieves the best performance when using less than 64 array antenna elements. On the other hand, FFT alone can provide high accuracy when using an ultra massive antenna system (e.g., 256,512,1024). Additionally, the findings observed the effect of key parameters on the performance of AoA algorithms, such as low SNR, a small number of snapshots (samples), and the effect of multipath signals.

SUBJECT AREA: π.χ. Wireless Communication

KEYWORDS: π.χ. Angle of Arrival, AoA, Direction Finding, positioning, 5G

(ACKNOWLEDGMENTS)

This Master Thesis has been accomplished in the framework of the European Funded Project: **SMART Telecom and Sensing Networks (SMARTNET)** - Erasmus+ Programme Key Action 1: Erasmus Mundus Joint Master Degrees – Ref. Number 2017 – 2734/001 – 001, Project number - 586686-EPP-1-2017-1-UK-EPPKA1-JMD-MOB, coordinated by **Aston University,** and with the participation of **Télécom SudParis, member of IP Paris** and **National and Kapodistrian University of Athens.**

Special thanks to Dr. Dionysis Xenakis, my technical advisor, for guiding me and supporting me during my thesis writing. I would also like to express my gratitude to my supervisor, Dr. Nikos Passas, for the opportunity to work on this topic.

I would like to express my deep gratitude to Dr. Stylianos Sygletos for managing the SMARTNET program and for being so kind to us. Additionally, I appreciate the assistance of the program's administrative staff Tanya, Zorina, and Isabel, during the two years.

Also, I am grateful to all my family members and my fiancée for their endless support during my studies.

CONTENTS

LIST OF FIGURES

LIST OF TABLES

1. INTRODUCTION

Radio-based positioning (aka localization) has long been utilized for tracking and navigation applications. Global Navigation Satellite Systems (GNSS) were and continue to be the main positioning technology where it originated by offering a service for military purposes and later expanded to include civilian uses. Despite the fact that many GNSS systems are now accessible, and the majority of terminals support hybrid GNSS systems such as GPS and GLONASS, the service still has limits for certain applications (e.g., indoor positioning). Moreover, given its accuracy limitation, GNSS is incapable of meeting the needs of future applications such as autonomous driving and industrial robots in indoor scenarios. In the European GNSS, GALILEO, the accuracy is one meter for the premium users and five meters for the regular users [1]. Several technologies are being studied to achieve indoor positionings, such as Wi-Fi-based localization, Bluetooth-based localization, and Visible light communication. Although these techniques can achieve a good level of accuracy, they are still limited in the indoor environment.

In contrast, the 3rd Generation Partnership Project (3GPP) suggests that the accuracy should be in the tens of meters for emergency calls, a few decimeters for indoor applications, and one decimeter for vehicle-to-everything (V2X) use cases [2], [3]. This degree of precision will emerge in many applications dependent on localization, and new technologies in 5G and beyond networks assist in improving this degree of accuracy in the positioning. For instance, 5G new radio (NR) offers a considerable bandwidth, high carrier frequency, and massive antenna array. These technologies are an excellent opportunity to enhance the positioning accuracy to meet the requirements of nowadays applications and services. In beyond 5G NR and for 6G, new technologies will improve the positioning accuracy by using more high-frequency range at THz ranges and much larger bandwidths[4] and using Reconfigurable Intelligent services (RIS) and Machine Learning algorithms [5].

For a long time, the positioning service was integrated and utilized in the cellular network to fulfill the needs in the event of an emergency call. In the United States, these standards were regulated by the Federal Communications Commission (FCC). For example, enhanced 911 (E911) location criteria were established [6]. Moreover, positioning can play an essential role in network optimization, such as in network management and radio configuration spectrum, called location-aware communication. For example, the base station can steer the beam toward the desired user by localizing the user.

Generally, to study positioning, two stages need to be considered. First is the positioning measurements, which are the extracted information from radio frequency signals (RF), for example, Angle of Arrival (AoA), Time Difference of Arrival (TDoA), and Received Signal Strength (RSS); these measurement methods require specific algorithms and optimization methods. The second stage is the positioning methods, which are the methods that use the positioning measurements to calculate the desired object location, for example, Proximity and Triangulation.

The Angle of Arrival, or more often referred to as the Direction of Arrival (DoA), is a well-studied subject that is utilized in positioning techniques. Many algorithms were proposed to solve direction-finding; however, their performance is different and depends on many parameters, such as signal-to-noise ratio (SNR), the number of snapshots (aka samples), and the number of antenna elements.

The thesis investigates some of the available traditional algorithms and their mathematical model, performance, complexity, and the possibility of using them in a 5G network according to the use cases. A CASCADE algorithm is proposed to benefit from one of the super-resolution methods while simultaneously reducing the complexity. The

algorithms' input signals were selected to be aware of the actual wireless communication environment. The signals are multipath signals with arbitrary attenuation and delay produced as duplicates of the line-of-sight component. As the primary signal for testing the algorithms, a sounding reference signal (SRS) was generated according to 3GPP standards.

The remainder of the thesis is organized as follows: **Section 2** discusses 5G positioning. **Section 3** will provide an introduction to the array signal processing and how to develop a mathematical model for estimating the Angle of Arrival. **Section 4** presents a study and comparison of Angle of Arrival methods. **Section 5** will include the simulation and results; **section 6** will conclude the thesis with a discussion and recommendations for further study.

2. POSITIONING IN 5G NETWORK

The new generation of mobile communication (5G) delivers new methods and technologies as enablers for positioning to achieve accuracy close the meter and centimeters according to the use cases. Massive MIMO, mmWaves, and Hybrid beamforming are good examples of 5G NR capabilities considered a new opportunity for positioning. 5G provides not only enablers for precise positioning as such but also introduces some new positioning methods. Positioning based on multi-cell round trip time (multi-RTT) measurements, multiple antenna beam measurements to enable downlink angle of departure (DL-AoD), and uplink Angle of Arrival (UL-AoA) estimate have been introduced as new concepts[7]. TR 38.913 in 3GPP specifications gives for the first time in section 9.2 an outlook on the actual realization of 5G positioning[8].

This section briefly discusses the positioning measurement methods in 5G. The second sub-section will discuss the enabling technologies in 5G that may be utilized to substantially improve localization by improving Angle of Arrival Estimation, which is the primary focus of this thesis. The third sub-section will discuss the 5G positioning architecture. Subsection four will discuss positioning signals in 5G. At the end of this section, use cases for 5G network localization will be presented.

2.1 Positioning Measurement Methods

As mentioned earlier, positioning measurement methods are used to extract information from the radio signal to be used for positioning algorithms to localize the user by using one of the positioning methods, for example, the triangulation technique. Six new or reformed techniques have been included into TS 38.305 in 5G NR specifications[9], [10] as follows:

a. Time-Based methods:

1. Downlink- Time Difference of Arrival (DL-TDoA)
2. UpLink- Time Difference of Arrival (UL-TDoA)
3. Multi-Round Trip Time (Multi-RTT)

b. Power-based methods:

4. New Radio Enhanced Cell ID (NR E-CID)

c. Angle-based methods:

5. Downlink – Angle of Departure (DL-AoD)
6. UpLink- Angle of Arrival (UL-AoA).

The methods listed above will be discussed briefly in this subsection, and the emphasis will shift later in the thesis to UL-AoA.

2.1.1 Time Difference of Arrival (TDoA)

TDoA measures the time lapse between receiving signals from two different transmitters [11]. **Eq.2.1** shows how TDoA is measured.

$$\boldsymbol{TDOA = T_{r2} - T_{r1}} \qquad (\mathbf{2.1})$$

Where,

$\boldsymbol{T_{ri}}$ is the time when the signal from source i is received.

From that time difference, the difference in the distance between each source and receiver can be calculated by Eq.**2.2**.

$$(\boldsymbol{d_2 - d_1}) = (\boldsymbol{T_{r2} - T_{r1}}).\boldsymbol{v_p} \qquad (\mathbf{2.2})$$

where,

$\boldsymbol{d_i}$ is the distance between the receiver and the ith transmitter.

When using the TDoA method, the receiver does not need to know the exact time of sending the signals from the base stations (gNBs). As a result, the receiver is not required to be synchronized. However, the timing difference between the transmission of the two signals (i.e., time offset) must be known. As a result, the transmitters must still be synchronized with one another. A synchronization error between the gNBs will cause a TDoA measurement error, as shown by **Eq.2.3** where $\boldsymbol{\tau_{ti}}$ is the clock bias of transmitter $\boldsymbol{i}$.[12]

$$\boldsymbol{TDOA = T_{r2} - T_{r1} - \tau_{t2} + \tau_{t1}} \qquad (\mathbf{2.3})$$

After collecting the measured data, the distance between the target and two different base stations may be calculated using the preceding equation. In this instance, a set of hyperbolic equations can be constructed, and the solutions correspond to the user's coordinates.

In general, iterative, analytical, and search techniques are among the most frequently used algorithms for problem-solving [13]. Because the equations derived from the TDoA technique are nonlinear, solving them is complicated and challenging, and much research has been conducted to determine the best way to resolve this problem.

DL-TDoA is the successor technology to LTE's OTDOA method. It operates on a similar basis to that explained earlier. However, in DL-TDoA, the user locates itself passively without reporting and sending information to the network. The mobile device calculates the time interval between the receipt of location signals from several gNBs. UL-TDoA operates in the same manner as DL-TDoA, except that the time difference measurements are performed via a network of base stations.

2.1.2 Multi-Round Trip Time (Multi-RTT)

A round-trip time (RTT) measurement is a kind of Time of Arrival (ToA) measurement. RTT estimates when a signal is sent and when the response or acknowledgment to that signal is received back. As a result, the RTT measurement is two times the ToA value in the ideal situation. It is not necessary to have synchronization between the gNB and the UE since both the initial signal transmission and the acknowledgment receipt are performed at the same device using the same clock, as indicated in **Eq.2.3**,

where, $\boldsymbol{T_{t,s}}$ is the transmission time,

$\boldsymbol{T_{r,acl}}$ is the acknowledgment time,

and $\boldsymbol{\tau_t}$ is the clock bias of the transmitter.

$$\boldsymbol{RTT = \left(T_{r,ack} + \tau_t\right) - \left(T_{t,s} + \tau_t\right) = T_{r,ack} - T_{t,s}} \qquad (\mathbf{2.3})$$

An extra error can be caused by the receiver's processing time (i.e., the time between receiving the signal and receiving the acknowledgment). This processing time results in a delay that is added to the RTT measurement. The processing time may be computed or approximated and deducted from the overall measurement. This was done in LTE, for example, for ECID measurements. [12]

One of the drawbacks of RTT in LTE ECID is that it only allows UE Rx-Tx measurement in relation to the serving base station. The distance to neighbor base stations required for a trilateration method can only be calculated via power measurements, often inaccurate. This issue was addressed in 5G NR by adding a new positioning technique known as multi-RTT. This technique also provides a process for performing RTT measurements on neighboring base stations, allowing the trilateration algorithm to use just timing data. For NR, the 3GPP opted to keep both approaches separate: Multi-RTT refers to a technique that utilizes multiple RTT measurements to both serve and neighbor base stations, while NR ECID only relates to power measurements to neighbor cells.

2.1.3 New Radio Enhanced Cell ID (NR E-CID)

The NR ECID technique differs substantially from what was known as ECID in LTE. To begin with, NR ECID is only reliant on power measurements, as defined in TS 38.305 [9]. The RTT measurement is now part of a multi-RTT positioning correction and is no longer part of the NR ECID method. A second significant distinction is that the mobile device is not required to perform for NR ECID. Besides, the mobile device is not required to conduct any particular measurement in the NR ECID method. However, It reports any information that is already accessible at the time of the request.

2.1.4 Downlink – Angle of Departure (DL-AoD)

Angle-based positioning is supported by 5G NR, particularly with mm-waves, and it is expected to give promising results. The concept of Angle based positioning is to find the direction of the beam transmitted from the gNB towards the user in the DL-AoD method and vice-versa in the UL-AoA method. In the simplest Scenario for an explanation, if the user receives three signals from 3 gNBs, that user's location can be determined using the DL-AoD method's triangulation technique, as shown in **Figure 2.1**.

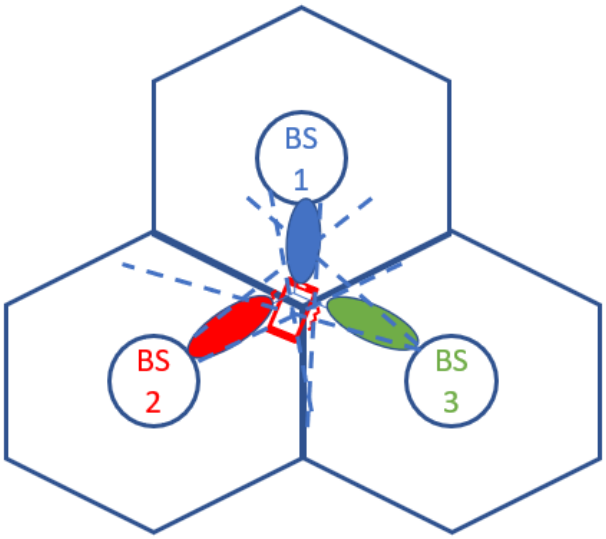

Figure 2.1: DL-AoD method

Each beam of the base station in 5G NR is assigned a beam index, which allows the mobile device to distinguish between the various beams. The downlink positioning reference signals from various beams received by the mobile device are measured by DL-AoD[9]. The measurement of the position in DL-AoD is performed by the mobile device and reported back to the network. Thus, the positioning is achieved on the UE without needing the uplink transmission.

2.1.5 UpLink- Angle of Arrival (UL-AoA)

The concept of AoA is to use an array antenna system to extract the phase information from signals impinging on the antenna elements, and that phase contains the information of the Angle of Arrival. The Angle of Arrival is considered an essential part of many applications in positioning. Moreover, it can assist in communication, for example, assisting DL-beamforming for steering the beam toward the user. This measurement method is the opposite of that one in DL-AoD, where the base station in the AoA method identifies from which direction the uplink signals of the mobile device are coming by using

beamforming or some algorithm that will be discussed later in section 4. Section 3 will explain in detail how AoA can be estimated, and then in section 4, further study will be conducted on the different algorithms that can be used for the estimation.

2.2 5G Positioning methods

Positioning technologies are generally split into three categories: triangle relationship positioning technology, scene analysis positioning technology, and proximity relationship positioning technology[14].

- **Positioning technology based on the triangle relationship**: Based on the measured data, this positioning technology calculates the location of the measured item using the geometric triangle or hyperbola connection. It is the most commonly used and essential positioning technique.
- **Scene analysis-based positioning technology**: This positioning technology abstracts the particular positioning scene, characterizes each place in the scene with precise and quantitative characteristics and combines the information into a database. Within the industry, such quantized location feature information is known as a signal "fingerprint," and it is compared to the information in the database to identify the position of the item based on particular matching criteria.
- **Proximity-based positioning technology**: This positioning technology predicts the location based on a proximity connection between an item to be located and one or more known location reference points. This technique often needs the aid of an identification system, and each known location is assigned a unique identity. A cell ID in a mobile cellular communications network is the most frequent example.

2.3 5G NR enabler technologies for positioning

Compared to earlier generations of mobile communication, 5G NR brought additional capabilities to enhance positioning accuracy. Among these capabilities are mm-waves and the large bandwidth, massive MIMO and beamforming, and network densification[8]. These new technologies are an excellent opportunity for positioning. It can be said that any improvement in communication gives a new opportunity for improving the localization. This sub-section will present some of the new technologies in 5G NR that will directly enhance the positioning.

2.3.1 mm-waves and high bandwidth

5G NR is designed to enable deployment over a broad frequency range. The 3GPP has specified two 5G operational frequency bands[15]:

- FR1: 450 MHz – 6,000 MHz (sub-6 band)
- FR2: 24,250 MHz – 52,600 MHz (mm-waves band)

The high bands over 24 GHz (FR2) in the spectrum were chosen in 5G because they have the ability to handle huge bandwidths, making them suitable for expanding the capacity. Because of the small wavelengths that can be measured in millimeters, "mm-waves" are used to describe these high-frequency bands. The mm-waves bands stretch up to 300 GHz. The bands from 24 to 100 GHz are expected to be used for 5G and beyond.

Previously, using frequency ranges far above 6 GHz was thought to be inappropriate for mobile communications owing to significant propagation losses and the signals are often obstructed not just by buildings and plants but also by the human body. Despite these challenges, emerging antenna technologies and a better knowledge of channel

characteristics and signal propagation allow for a range of deployment alternatives to be investigated. **Figure 2.2** indicates the frequency bands in 5G.

Because frequencies may be reused over relatively short distances, the smaller cell sizes of 5G mm-waves offer excellent throughput and allow for efficient spectrum utilization. Outdoor cell sizes are expected to range from 100m to 200m, while indoor high-density deployments may be as tiny as 10m.

This increase in bandwidth and frequency has a twofold impact on the positioning. Larger bandwidths provide for better delay resolution, allowing for the estimation and tracking of the multipath signals. The high-frequency leads to "optical-like propagation" and reducing the effect of shadowing and diffraction[16].

In the sub-6 GHz, carrier aggregation can also increase the bandwidth; nevertheless, more dominant multipath signals will exist. This increase in bandwidth will aid in improving time estimate resolution, providing yet another possibility for improved positioning.

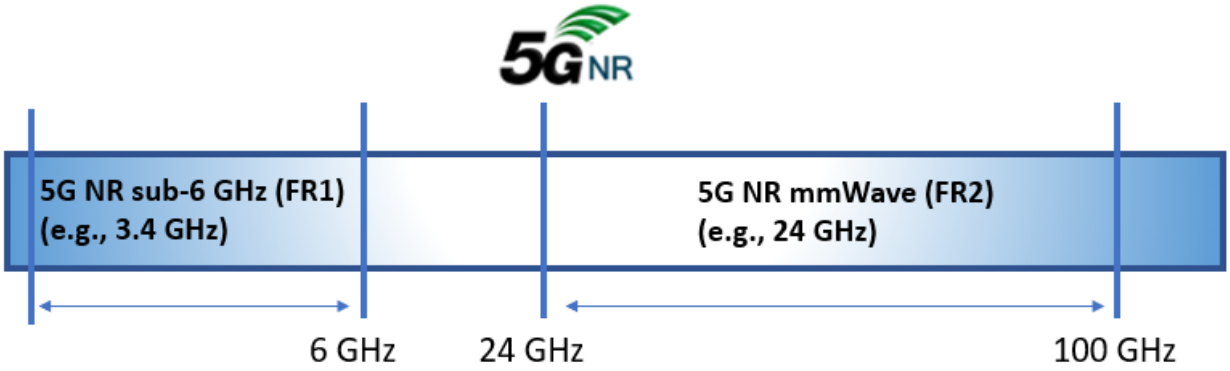

Figure 2.2: 5G NR Frequency Bands

2.3.2 Massive MIMO and Beamforming

Increasing carrier frequencies leads to shorter wavelengths ($\lambda = \frac{c}{f_c}$), which allows more antennas to be used in a given space[17]. Massive MIMO antennas generate highly directed beams that concentrate transmitted energy to overcome path losses and non-line of sight (NLOS) situations.

Due to the short wavelengths associated with mm-waves, even large MIMO antennas may be relatively compact, and tiny effective antennas can readily be incorporated into consumer devices. Whereas MIMO antennas operating at less than 6 GHz may support up to eight elements, massive MIMO antennas operating at mm-waves frequencies may support up to 128, 256, or more elements. In beyond 5G, it is expected to use a new portion of RF spectrum which is in Terahertz (THz), and these frequencies might support more antenna, e.g., 1024 × 1024 in ultra massive MIMO [18].

Not all RF channels will contain ADCs (Analog to Digital Convertors) to limit the power consumption. Thus, this massive number of antennas will handle only a few streams. A mix of digital and analog beamforming will be used to convert feeds to antennas[8]. This massive number of antennas with the beamformer capabilities will make Angle-based positioning possible and significant in 5G and beyond, especially in FR2, as the beams are narrower and directive. This is shown in **Section 5** of the thesis, where a scenario is used to assess the Angle of Arrival algorithms' performance as the number of antenna elements grows.

Figure 2.3 shows 1024 × 1024 ultra Massive MIMO.

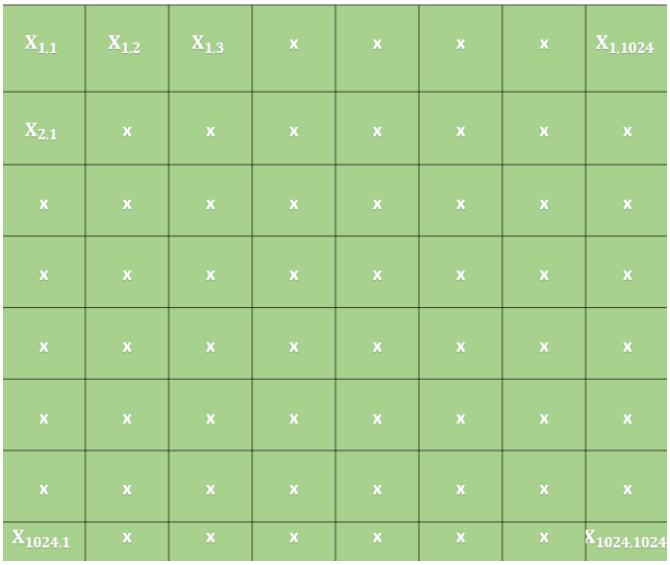

Figure 2.3: 1024 × 1024 ultra Massive MIMO.

Figure 2.4 shows how the beamforming with MIMO antennas can be used to focus the beam toward the desired user.

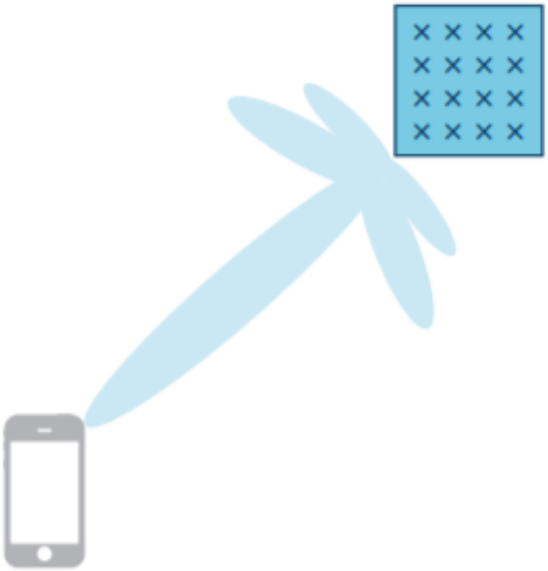

Figure 2.4: Beamforming with MIMO [19]

Angle-based positioning techniques are made possible by these features in 5G. Angle-based techniques may offer very high positioning accuracy in FR2 due to the large antenna.

2.3.3 Dense Network

5G networks will be considerably denser than previous network technologies. According to some estimates, 5G would need the installation of up to 20 base stations in areas where 4G could serve with only one [20]. In ultra-dense networks, the distance between gNBs is short, and the distance between the gNB and the UE is also short. This is excellent for positioning since it improves the chances of having a direct line of sight. For example, for ranges between 5 and 50 meters, that chance may be 50% [21]. This will assist in better estimation for the Angle and the delay.

3GPP TR37.913 [22] gives deployment Scenarios with different frequency bands and the number of antennas. Examples from those Scenarios are shown in **Table 2.1**.

Table 2.1: Deployment Scenarios in 5G

Frequency	BandWidth	BS Antenna	Scenario
700 MHz	20 MHz	64	Rural
700 MHz	40 MHz	64	Extremely long distance
700 MHz, 2.1 GHz	40 MHz	4	Urban for mMTC
4 GHz	200 MHz	256	Dense urban, rural, urban macro, high speed
6 GHz	200 MHz	256	Highway, connected cars
30 GHz	1 GHz	256	Dense urban, urban macro, high speed, indoor spot
70 GHz	1 GHz	256	High Speed, indoor spot

2.4 5G architecture for Positioning

The 5G positioning architecture is defined by 3GPP, as illustrated in **Figure 2.5**. The UE, the 5G RAN (NGRAN), and the core network comprise the 5G localization system. Using the benefits of 5G network infrastructures, operators may combine 5G positioning capabilities with the communications network to provide both 5G network communications and positioning services.

Figure 2.5 shows the 5G architecture that supports the positioning. It can be seen from the Figure that there is a new entity called "LMF," which stands for Location management function. This new entity gets the information and measurement from the Radio Access Network (New generation RAN NG-RAN), which collects in its turn the information from new generation node B (gNB) and the user equipment (UE).

This information is delivered to the LMF by AMF, which stands for Access and Mobility management function. The interface between AMF and LMF is the NLs interface. The Figure shows that the positioning information is carried by a new positioning protocol (NRPPA) over the NG-C, which is the control plane interface.

These improvements to the 5G network give the foundation for 5G localization. The LMF contacts the UE through AMF utilizing the LPP (LTE positioning protocol). The NG RAN contacts the UE via LTE-Uu and NR-Uu utilizing the RRC (radio resource control protocol) [23].

The user can report the location information to the network and also can send the SRS (sounding reference signal), which assists in the localization measurement (channel estimation). While the network side by the gNB sends the positioning reference signal (PRS). These two signals will be explained in the next sub-section.

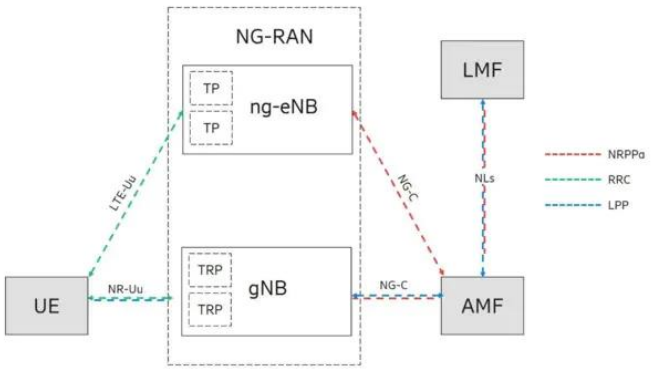

Figure 2.5: 5G architecture supporting Positioning [23]

2.5 5G positioning signals

Two reference signals are in the 5G NR specification dedicated for positioning. In the downlink direction (i.e., From gNB to the UE), a positioning reference signal (PRS). In the uplink direction (i.e., from the UE to the gNb), a sounding reference signal (SRS).

2.5.1 New Radio Positioning Reference Signal (NR PRS)

PRS is the primary reference signal for positioning techniques that rely on downlinks (DL). While other signals may be used, PRS strives to offer the greatest level of accuracy. Furthermore, it provides very good coverage and interference avoidance.

The available reference signals in DL, such as the channel status information reference signal and the synchronization signals, are not utilized for location estimation [24] because of interference from neighboring cells when signals from several cells collide in both the time-domain and frequency-domain, these reference signals are incapable of identifying a significant number of gNBs. Because of this interference, signals from close cells shadow the weak signals from distant cells, making it harder for the UE to identify distant cells or gNBs. As a consequence of this problem, hearability suffers [24].

PRS overcomes these mentioned limitations with a new technique called "Muting." Multiple cells transmit the PRS in a coordinated way using PRS muting, which prevents interference from neighboring cells by muting the relevant PRS transmission instances.

The comb size refers to the number of subcarriers occupied in a particular PRS symbol. For comb-2,4,6, and 12, many customizable comb-based PRS patterns are appropriate for various situations and use cases. The pattern shown in **Figure 2.6** is the comb size of six, with three base stations multiplexed over a single slot period. N symbols may be merged in comb-N PRS to encompass all subcarriers. To prevent interference, each base station may broadcast in separate sets of subcarriers. This method is also latency efficient since many base stations may broadcast at the same time without interfering with each other.

2.5.2 New Radio Sounding Reference Signal (NR SRS)

SRS is an uplink reference signal sent from the UE to the gNb. SRS assists in channel estimation by the concept of sounding where the SRS signal is unique, and the base station has a pre-knowledge of the SRS signal. This pre-knowledge helps to estimate the delay at the receiver. It plays an important role in channel estimation, especially in TDD (Time Division Duplex), benefiting from channel reciprocity.

An NR-SRS is an uplink orthogonal frequency division multiplexing (OFDM) signal generated with a Zadoff–Chu sequence on different subcarriers, as specified in 3GPP TS 38.211 [25].

In 3GPP Release 16, the SRS for the location was added in the uplink direction. This new signal addresses two positioning-related issues [23]:

- Because positioning needs measurements from several receiving base stations, the new signal must have enough range to reach the serving base station to which the UE is connected as well as the surrounding base stations participating in the positioning process.
- The SRS is likewise built to span the whole bandwidth, with resource elements distributed over several symbols to cover all subcarriers.

Similar to PRS, SRS is based on a comb pattern. By allocating various comb patterns to UEs, they may be multiplexed over the same transmitting symbol. **Figure 2.6** depicts an example of SRS by a UE.

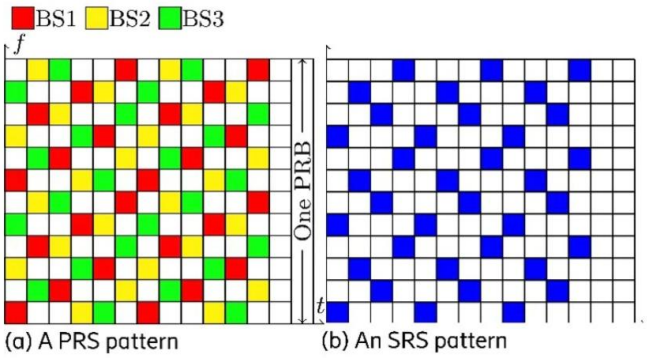

Figure 2.6: PRS and SRS configuration

In 5G NR frames, there are two stages to generating the SRS [26], Zadoff–Chu sequence and Mapping to OFDM symbols. Zadoff–Chu sequence is a complex-valued sequence created by shifting a root ZC sequence cyclically. ZC sequences offer a variety of appealing characteristics, which is why they are employed for estimating the channel:

- These sequences have a constant amplitude. This guarantees optimal power amplifier usage. This feature is crucial for the uplink transmission since that the UE has a limited battery [27].
- The most important feature is for the same root zadoff sequence; zero is the cross-correlation between various cyclically shifted sequences, which is the most significant characteristic. This implies that the base station will be able to segregate users and eliminate interference [27].

Furthermore, the orthogonality of the SRSs from various UEs gives perfect situations for positioning methods to identify, locate many users [26]. The users can be separated, which means interference can be avoided with this feature. **Figure 2.7** shows the correlation results between SRS signals with different cyclic shifts. It can be seen from the Figure that the correlation result is zero when the cyclic shift is different.

5G NR SRS configuration is explained in the below points with highlighting the differences with SRS LTE [28]:

- Max SRS symbols can be 1,2, or 4 $\boldsymbol{N_{Sym}^{SRS}} \in \{\mathbf{1}, \mathbf{2}, \mathbf{4}\}$**,** while in LTE, the max number of symbols is one. Thus, 5G NR SRS has a better sounding capacity in comparison with LTE.
- Symbol number for SRS transmission depends on $\boldsymbol{I_{offest}}$, where $\boldsymbol{I_{offest}}$ is the time domain starting position, while in LTE, it is always transmitted at the last symbol of the slot.
- SRS transmission is flexible. It depends on transmission comb size $\boldsymbol{K_{TC}}$ **= {2,4}**. In LTE SRS, the comb size is only 2.

- The Max number of cyclic shifts can be 12. Hence, max 12 UEs can transmit SRS simultaneously using one antenna port. However, in the LTE max number of cyclic shifts are 8. Hence, 8 UEs can transmit SRS simultaneously using one antenna port.

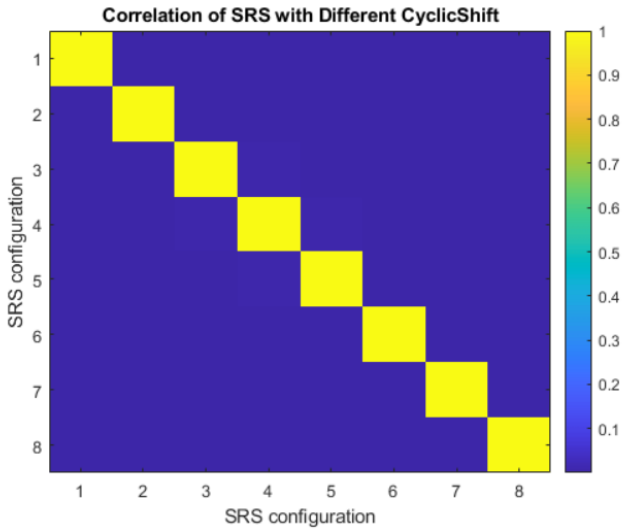

Figure 2.7: Correlation between SRS signals

2.6 5G Positioning Use Cases Requirments

With 5G's presence in a wide range of applications comes a wide range of needs. **Figure 2.8** depicts the developing criteria and how they correspond to 3GPP Releases [10]. The latency and horizontal positioning error are the two main indicators that we concentrate on here. For regulatory use cases, horizontal accuracies of less than 10 meters were required for 80 percent of users in outdoor applications. In contrast, for additional Release 16 (Rel-16) commercial use cases, horizontal accuracies of less than 10 meters were required for 80 percent of users in outdoor applications. For 90% of devices in Rel-17, the goal performance for Industrial Internet of Things (IIoT) use cases is 20 centimeters horizontal positioning precision and less than 1-meter vertical positioning accuracy [10].

It can be seen from the Figure that not only the accuracy, which is important for the use cases, however, but the latency is also of great importance. For instance, the accuracy is down to one meter for augmented reality, and the latency should be around 15 ms. For Inbound logistics for driving trajectories, the accuracy is within 30 cm, and the latency is 10 ms.

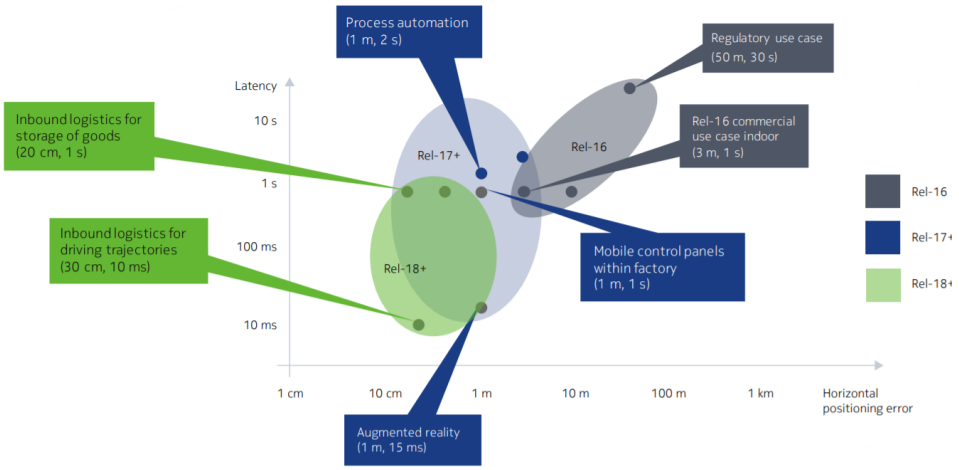

Figure 2.8: Use Cases Requirements for 5G positioning [10]

3. Array Signal Processing

In recent decades, much attention has been paid to the area of array signal processing (ASP), and many researchers are still delving deeply into its various domains, particularly signal direction finding or estimation of the Angle of Arrival, with the goal of improving accuracy, resolution, increasing the degree of freedom, and reducing the complexity of the algorithms. In cellular communication systems, AoA estimate can be utilized to optimize downlink transmission efficiency. Because the propagation channel geometry remains constant in terms of AoAs, paths, and average power, detecting and estimating the DoA in the uplink assists the design of a beamformer in the downlink. In 5G NR as mentioned in the previous section has included AoA measurement as a positioning method in 5G NR to be used for enhanced positioning.

This section will cover the fundamentals of Array Signal Processing and Smart Antennas, which will serve as the basis for our work on estimating the Angle of Arrival. The section will begin with introducing smart antennas and their classifications; after that, the section will discuss the spatial spectrum estimation system. The array antenna and the Angle of arrival concept will be discussed at the end of this section.

3.1 Smart Antenna

Before diving in-depth into how to estimate Angle of Arrival (AoA) and explaining the different types of algorithms for such purpose, it is crucial to show the basics of array signal processing which is the primary concept that will be applied for the system model of AoA estimation. Smart Antennas have been considered one of the leading technologies in wireless communication that achieves a high efficiency of communication and maximizes the capacity significantly, particularly in dense areas, by adaptively filtering out interference while focusing on the particular recipient [22]. As in recent years, Smart antenna paid much attention to researchers and engineers, which gives much flexibility in shaping the beam and searing it in the appropriate direction to increase the transmission efficiency.

Smart antenna technology may be categorized into three types, which are described in more detail below [29] :

1. **Switched lobe (SL):**
   This straightforward method comprises a basic switching function between the array's predefined beams. Among the remaining beams, the one that performs the best (typically in a received power) is selected.
2. **Dynamically with phased array (PA):**
   The premise of this technique is to allow continuous tracking of the signal sources by employing algorithms for the Angle of Arrival (AoA) estimation in the system. Therefore, the transmission is smarter in this technique where it is based on the AoA.
3. **Adaptive array (AA):**
   In the Adaptive array (AA) technique, the beam pattern is adjusted to null out the interferers, which can be located by using DoA algorithms; however, the received power from the wanted direction is maximized. The Adaptive Array uses the AoA algorithm to find both directions of the interference sources and the desired signal.

   Due to the fact that we are attempting to estimate the Angle of Arrival, which is essentially done on the receiver side, the basic architecture of the Smart receive antenna will be described. It is composed of three major components, as shown in **Figure 3.1**[29]

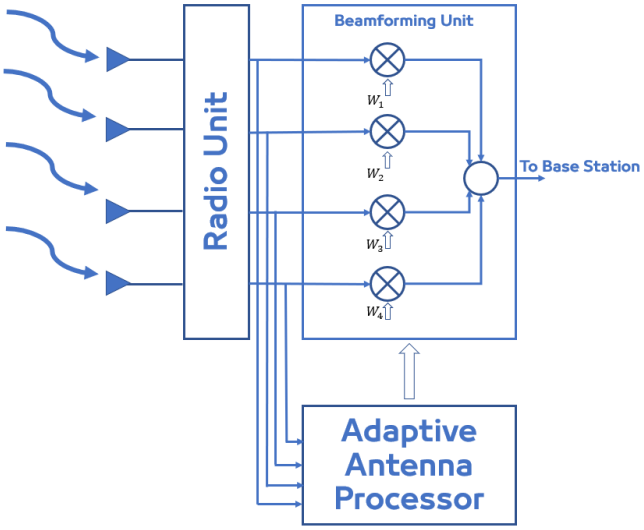

Figure 3.1: Smart antenna receiver

- **Radio unit:**
  This unit is responsible for capturing the RF signals using the array antenna system; then, the received signals will be downconverted from high frequency to the baseband frequency (i.e., remove the carrier). Finally, the received signals are converted to a digital signal using analog to digital converters (AD) for further processing. It is essential to mention here that for the analog array, the radio unit consists of physical phase shifters for each channel (RF chain) and only one AD; however, the digital array has AD for each RF chain.
- **Beamforming unit:**
  This unit accomplishes the forming of the beam in the desired direction. The weights are added to the received signals, and then the total signal is calculated using the following equation.

$$\boldsymbol{y(\theta_i) = \sum_{m=0}^{M-1} w_m^i \, x_m} \qquad (3.1)$$

Where,

$\boldsymbol{y(\theta_i)}$ is the output of a beamformer,

$\boldsymbol{x_m}$ is the sampled mth array element received signal,

$\boldsymbol{w_m^i}$ is the weight vector which used to form the beam at angle $\boldsymbol{\theta}$, or to null it at Angle $\boldsymbol{\theta}$

and $\boldsymbol{M}$ represents the number of antenna elements.

- **Adaptive antenna processor (AAP):**
  This unit is responsible for determining the complex weights for the beamforming unit. This unit consists of several stages, such as Angle of Arrival estimation and Weight generation.

The direction of Arrival (DoA) is another term used to describe the direction of the signal or the Angle of Arrival (AoA). This thesis will focus on the AoA/DOA estimator, which is considered the most important part of the (AAP). Many AoA algorithms such as Multiple Signals Classification are used to estimate the Angle of Arrival that we aim to employ for positioning purposes.

3.2 Spatial Spectrum Estimation System

The spatial spectrum is a major issue in many use cases, including radar, sonar, astronomy, and positioning. It is described as the amount distribution of the energy for the signals with respect to all directions. Therefore, the spatial spectrum estimate is also known as the direction of arrival estimation [30].

While the Fourier transform (e.g., Fast Fourier Transform) may be used to get the frequency spectrum of a received signal, the spatial spectrum has its own techniques. The spatial spectrum is obtained using these techniques by estimating the Angle of Arrival (AoA). Intuitively from the name of the spatial spectrum, the idea is to divide the space and identifying the signals by their angles (i.e., AoA). Three stages comprise the spatial system: the target stage, the observation stage, and the estimate stage, as shown in **Figure 3.2** [31].

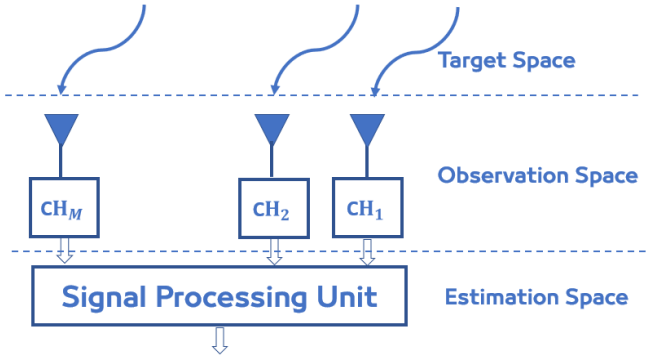

Figure 3.2: The system structure of AoA spatial spectrum estimation

- **The target space:**

  This stage includes the characteristics from the source signal as well as the complex surroundings, such as noise, that may affect the sent signal.

- **The observation space:**

  The signal characteristics are observed in this stage, such as azimuth, elevation, distance, and polarization. This observation will include the undesired signals due to the complex environment, such as inference and noise. Moreover, the array antenna element may influence the observation as it contributed to the collected signal. Therefore, channel inconsistency, frequency band inconsistency, and the impairment of mutual coupling between antennas might affect the observation of the characteristics of the received data.

- **Estimation space:**
  Mainly, the function of the estimation space is to reconstruct the targe stage. In this stage, the signal characteristics are extracted from the complex environment using array signals processing techniques, such as MVDR or MUSIC. The main challenges in this stage are accuracy, resolution, and complexity. In addition, many factors affect the estimation, for example, the Signal to Noise ratio (SNR) and the correlated multipath signals.

3.3 Array Antenna and the principle of AoA

An array antenna is a collection of receive/transmit antenna components arranged in a certain shape (or even random distribution in some cases) to improve the antenna's gain and directivity. Currently, the aim is to utilize massive or even ultra-massive antennas, especially in mm-waves (the new range of frequency bands), to address the transmission impairments in wireless communication (e.g., propagation loss). Increasing the number of antenna elements, on the other hand, increases the system's complexity, as will be

shown later in **section 5**. Many array antennas are available for various applications; for example, linear array antennas are used to estimate a one-dimensional AoA (i.e., elevation or azimuth), while planner array antennas can be used to estimate a two-dimensional AoA (i.e., Azimuth and Elevation). Other kinds of array antennas include utilizing a virtual sub-array antenna to expand the aperture size of the antenna while maintaining the system's low complexity or using the idea of coprime array antenna to improve the estimation of Angle of Arrival.

The idea of using an array antenna for the Direction-finding applications is to extract information from the received signal itself by finding the difference in phase of the received signal at the $\boldsymbol{M}$ elements. To explain the process of estimation, let us consider, as shown in **Figure 3.3**, three antenna elements as a simple case distributed uniformly to construct a linear array antenna.

It can be seen from **Figure 3.3**, the impinging signals on the array elements arrive at different times as the signals impinge on the second and the third array element travel longer distances (i.e., phase difference). The rightmost element is assumed to be the reference element and numbered the first element, followed to the left second, and third elements. The distance between adjacent elements is $\boldsymbol{\Delta}$, and this parameter should be chosen carefully with its value to avoid what is so-called in antenna and propagation theory "grating lobes."

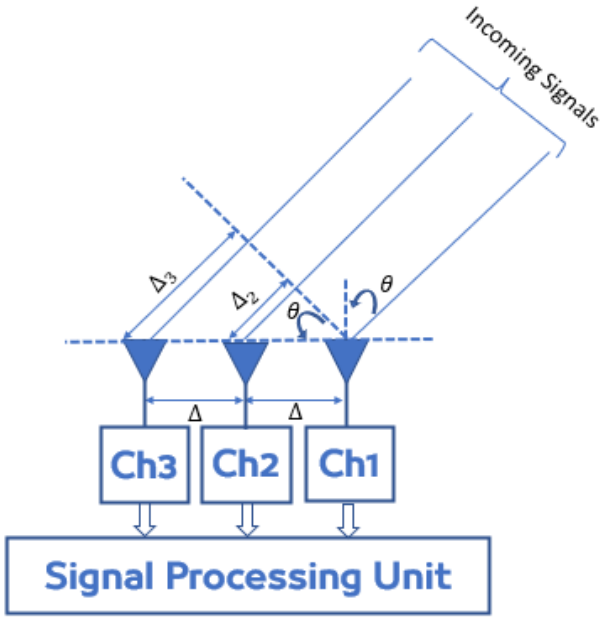

Figure 3.3: Three array elements

A basic assumption to develop the fundamental AoA data model is considering the far-field signals, which means that the three paths can be regarded as parallel, and this will simplify the dealing with geometric values that we are interested in (i.e., AoA). $\boldsymbol{\theta}$ here is the Angle of Arrival and $\boldsymbol{\Delta_m}$ is the further distance the signals take to arrive at the second and the third element, and it can be expressed as the following equation:

$$\boldsymbol{\Delta_m = (m-1)\Delta.\sin(\theta)} \qquad \boldsymbol{m = 1,2,3} \qquad \boldsymbol{(3.2)}$$

Where,

$\boldsymbol{m}$ is the index of the array element,

$\boldsymbol{\Delta}$ is the spacing between the elements,

and $\boldsymbol{\theta}$ is AoA.

The first element's received signal is written as:

$$\boldsymbol{x_1 = s(t)} \tag{3.3}$$

$\boldsymbol{S(t)}$ Represents the transmitted signal.

The signal at the second and the third elements can be expressed as follows:

$$\boldsymbol{x_2 = s(t)e^{-j\beta\Delta_2} = s(t)e^{-\frac{j2\pi\Delta}{\lambda}\sin(\theta)}} \tag{3.4}$$

$$\boldsymbol{x_3 = s(t)e^{-j\beta\Delta_3} = s(t)e^{-2\frac{j2\pi\Delta}{\lambda}\sin(\theta)}} \tag{3.5}$$

where,

$\boldsymbol{\beta}$ is $\frac{2\pi}{\lambda}$ is the phase shift constant,

$\boldsymbol{\lambda}$ represents the signal's wavelength

The term $e^{-j\beta\Delta_{\mathrm{m}}}$ in **Eq. 3.5** and **Eq. 3.5** is the phase introduced by the extra distance the signal traveled to impinge on non-reference elements [32].

All of the above can be put in a MATRIX form to generalize the expression:

$$\mathbf{X} = \begin{bmatrix} \boldsymbol{x_1(t)} \\ \boldsymbol{x_2(t)} \\ \boldsymbol{x_3(t)} \end{bmatrix} = \begin{bmatrix} \mathbf{1} \\ \boldsymbol{e^{-\frac{j2\pi\Delta}{\lambda}\sin(\theta)}} \\ \boldsymbol{e^{-2\frac{j2\pi\Delta}{\lambda}\sin(\theta)}} \end{bmatrix} \boldsymbol{s(t)} = \begin{bmatrix} \mathbf{1} \\ \boldsymbol{e^{-j\mu}} \\ \boldsymbol{e^{-j2\mu}} \end{bmatrix} = \boldsymbol{a(\mu)S(t)} \tag{3.6}$$

where $\mu = 2\frac{\pi\Delta}{\lambda}\sin(\theta)$ and $\boldsymbol{a(\mu)} = \left[1, e^{-j\mu}, \ldots\ldots, e^{-j2\mu}\right]^T$ It is often referred to as the response vector or array steering vector. For an $\boldsymbol{M}$ elements or sensors, it can be rewritten as:

$$\mathbf{X} = \begin{bmatrix} \boldsymbol{x_1(t)} \\ \boldsymbol{x_2(t)} \\ \boldsymbol{x_3(t)} \end{bmatrix} = \begin{bmatrix} \mathbf{1} \\ \boldsymbol{e^{-\frac{j2\pi\Delta}{\lambda}\sin(\theta)}} \\ \ldots \\ \boldsymbol{e^{-j(M-1)\frac{2\pi\Delta}{\lambda}\sin(\theta)}} \end{bmatrix} \boldsymbol{s(t)} = \begin{bmatrix} \mathbf{1} \\ \boldsymbol{e^{-j\mu}} \\ \ldots \\ \boldsymbol{e^{-j(M-1)\mu}} \end{bmatrix} \boldsymbol{s(t) = a(\mu)S(t)} \tag{3.6}$$

The expression above was derived by considering a linear array; however, the expression is applicable to any other array [29].

4. ANGLE OF ARRIVAL MEASUREMENT TECHNIQUES

The design of an algorithm to solve a particular issue is dependent on the kind of problem, the parameters, and the constraints that should be considered while developing that algorithm. In a Mobile network, it is always necessary to reduce the time consuming for reporting any information to the network or user, especially in the 5G network and beyond. The reason for that is many applications require a high-speed network in terms of latency and data rate. Similarly, when it comes to positioning in a 5G network, the algorithm should be chosen based on many criteria, including estimate accuracy, the resolution required to differentiate between multipath signals, and the time required to provide the desired output. To that aim, this section explains how to estimate the Angle of Arrival (AoA) by analyzing and comparing various methods available in the literature in terms of mathematical models. The algorithms are different from each other in their premise of estimating AoA. Some of them require extensive searching to construct the spatial spectrum; others can resolve AoA directly without searching, which leads to a significant reduction in time consumption. The number of samples taken from the received signal is of great importance to many algorithms; however, other algorithms are not significantly impacted by the number of samples.

This section will explain all stated above by investigating the different types of algorithms for AoA estimation. Additionally, a CASCADE technique is proposed in this section, which combines two of the traditional algorithms for AoA estimation. This algorithm is proposed to simplify one of the available super-resolution algorithms by using the fast FFT-based Angle of Arrival method as the first stage to find the initial range of AoAs. Then, the CASCADE system's second stage uses one of the super-resolution algorithms [33] to precisely estimate the AoA.

The section begins with defining the data model using a uniform linear array to illustrate our model's matrix representation and quantify the covariance matrix, which forms the basis of many algorithms' estimations. Some linear algebra techniques, such as singular value decomposition, are introduced in advance to demonstrate sub-space AoA techniques later in this section. The second sub-section discusses some classic and contemporary methods used to estimate AoA as well as the proposed CASCADE method.

4.1 Data Model in Uniform Linear Array

This section will consider a Uniform Linear Array (ULA) as shown and described in **Figure 4.1** for most algorithms; however, certain algorithms that require specific array antenna geometry will be explained separately. Some assumptions have been made for our data model, as are defined in the following points:

1. Wireless Medium: The medium is assumed as linear and isotropic. Isotropic medium means that the medium has the same physical properties in all the directions, while linear medium means that the signals can be superposed linearly. This assumption of linearity allows the superposition property to collect the impinging signals on the antenna elements. Moreover, when the system is isotropic, the waves' propagation is independent of the direction of the signals (i.e., DoA). [29]
2. The far-field assumption: for the $\boldsymbol{K}$ signals generated from different sources; the signals are impinging on the antenna elements as parallel.
3. The signals are assumed as a narrowband with the same carrier frequency, and they are uncorrelated; however, in the simulation section, all signals will be multipath signals, which means that the signals are correlated to check the behavior of the algorithms in a real scenario.

4. AWGN channel: With zero mean, the noise is uncorrelated with the signals. The noises have a variance σ_N^2 at all the array elements, and this noise is uncorrelated within antenna elements.

In ULA, the spacing between the antenna elements is equal, denoted in this thesis as **Δ**.

The distance will be assumed equal to $\boldsymbol{\lambda/2}$ to prevent the grating lobes, which increases the ambiguity of the estimation. The number of equally spaced antenna elements is $\boldsymbol{M}$ enumerated as $(\boldsymbol{0, 1, \ldots \ldots, M-1})$. $\boldsymbol{K}$ represents the number of narrow bands signals. It is assumed that these signals are uncorrelated and uncorrelated with the noise for the explanation purpose. Later, the effect of the correlated signals from the multipath signals in wireless communication will be explained in **section 5**.

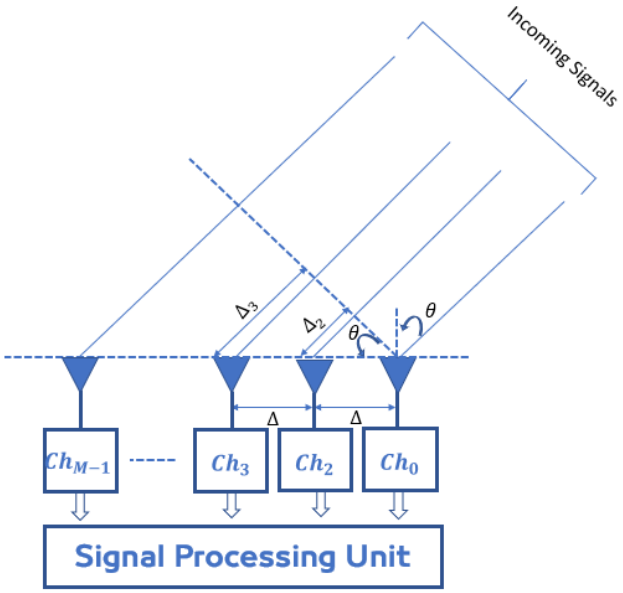

Figure 4.1: ULA data model

The received signal at $\boldsymbol{mth}$ element is expressed as:

$$\boldsymbol{x(t) = Real\{S_k(t) * e^{j2\pi f_c t}\}} \qquad (\boldsymbol{4.1})$$

where,$\mathbf{S_k}$ Is kth signal. As it was assumed previously, the signals are narrowband, which means **B** is less than $\boldsymbol{f_c}$ where **B** and $\boldsymbol{f_c}$ are the bandwidth and the carrier frequency, respectively. At each antenna element, the time delay can be straightforwardly calculated as:

$$\boldsymbol{\tau_m = \frac{m\Delta}{c}\sin(\theta)} \qquad (\boldsymbol{4.2})$$

Where $(\boldsymbol{m})$ is the index of the array element, and **Δ** is the distance between the elements of the array. This distance must be less than or equal to $\frac{\lambda}{2}$, as previously stated, to prevent ambiguity. $(\boldsymbol{\theta})$ is the Angle of Arrival to be estimated, $(\mathbf{c = \lambda f_c})$ is the propagation velocity, and $(\boldsymbol{\lambda})$ is the wavelength. It is important to note that we are ignoring any delay between the transmitting and receiving signals; hence at the first antenna (i.e., $\boldsymbol{m = 0}$) $\boldsymbol{\tau_m = 0}$. At mth element, the received signal is expressed as follows:

$$\boldsymbol{x_m(t) = Real\{S_k(t-\tau_m)\ e^{j2\pi f_c(t-\tau_m)}\}} \qquad (\boldsymbol{4.3})$$

The captured signal by the mth element is downconverted to the baseband for further processing; thus, the baseband received signal is:

$$\boldsymbol{x_m(t) = Real\{S_k(t-\tau_m)\ e^{-j2\pi f_c(\tau_m)}\}} \qquad (\boldsymbol{4.4})$$

After sampling, it becomes:

$$\boldsymbol{x_m(nT) = Real\{S_k(nT - \tau_m)\ e^{-j2\pi f_c(\tau_m)}\}} \quad (\mathbf{4.5})$$

Where, $\boldsymbol{T}$ is the sampling time.

Eq. 4.5 can be approximated due to the fact that $\boldsymbol{T}$ is larger than $\boldsymbol{\tau_m}$ [34].

$$\boldsymbol{T \gg \tau_m \ \ , \ \ m = 0, 1, \dots\dots\dots, M-1}$$

$$\boldsymbol{x_m(nT) = Real\{S_k(nT)\ e^{-j2\pi f_c(\tau_m)}\}} \quad (\mathbf{4.6})$$

It can be written in a discrete form as following:

$$\boldsymbol{x_m(n) = Real\{S_k(n)\ e^{-j2\pi f_c(\tau_m)}\}}$$
$$\boldsymbol{= S_k(n) e^{-\frac{j2\pi}{\lambda} m\Delta \sin(\theta)} = S_k(n) a_m(\theta)} \quad (\mathbf{4.7})$$

Where,

$$\boldsymbol{a_m(\theta) = e^{-\frac{j2\pi}{\lambda} m\Delta \sin(\theta)} \ for\ m = 0, 1, 2, \dots\dots, M-1}$$

For $\boldsymbol{K}$ signals, the superposition of the signals at one antenna element is expressed as follows:

$$\boldsymbol{x_m(n) = \sum_{k=0}^{K-1} S_k(n)\ a(\theta_k)} \quad (\mathbf{4.8})$$

for $k = 0,1,2, \dots . K-1$.

4.1.1 Matrix Representation

As the situation in mobile communication is to deal with many multipath signals, and each signal will be sampled with a sampling time which means more data to be processed, it is more convenient if a matrix form is considered when representing the model.

Eq.4.8 can be expressed now in a matrix form as follows:

$$\mathbf{X} = [\boldsymbol{a(\theta_0)}\ \boldsymbol{a(\theta_1)}\ \dots\dots\dots \boldsymbol{a(\theta_{K-1})}]\ \boldsymbol{S} + \boldsymbol{n} = \boldsymbol{AS} + \boldsymbol{n} \quad (\mathbf{4.9})$$

where,

$\mathbf{X}$ is the $\boldsymbol{M}$ x $\mathbf{N}$ matrix ($\mathbf{N}$ is the number of the samples or snapshots).

$\boldsymbol{A}$ is $\boldsymbol{M}$ x $\boldsymbol{K}$ matrix,

$\boldsymbol{S}$ is the received signal,

and $\boldsymbol{n}$ is AWGN.

Each column of $\boldsymbol{A}$ is a steering vector for a specific kth signal at different antenna elements. While each row of $\boldsymbol{A}$ is the steering vector of $\boldsymbol{K}$ signals at one antenna element, as shown below:

$$\boldsymbol{A} = \begin{bmatrix} \boldsymbol{a_0(\theta_0)} & \cdots & \boldsymbol{a_0(\theta_{K-1})} \\ \vdots & \ddots & \vdots \\ \boldsymbol{a_{M-1}(\theta_0)} & \cdots & \boldsymbol{a_{M-1}(\theta_{K-1})} \end{bmatrix} \quad (\mathbf{4.10})$$

4.1.2 Covariance Matrix

Distinguishing between desirable and unwanted signals is a critical stage in the AoA estimation process. Previously, it was assumed that noises are normally uncorrelated, contrary to signals, which are obviously correlated since they originate from the same sources. Practically, the noise distorts the signals collected by the antennas at the receiver (e.g., AWGN). This feature may be used to determine a method for obtaining the data required for direction finding.

Cross-correlation is the appropriate technique for this purpose. The covariance matrix measures the degree to which the data collected by array antenna elements is correlated. When the covariance matrix has a larger value, there is a higher correlation between the signals.

Most Angles of Arrival measurement techniques use the covariance matrix as a fundamental step in the algorithm.

The covariance matrix of the received data (i.e., signals and noises) is defined by:

$$\boldsymbol{R_{XX}} = \mathbb{E}[\mathbf{X}\mathbf{X}^{\mathbf{H}}] \quad (\mathbf{4.11})$$

$$= \mathbb{E}[(\boldsymbol{AS} + \boldsymbol{n})(\boldsymbol{AS} + \boldsymbol{n})^{\boldsymbol{H}}]$$

$$= \boldsymbol{A}\mathbb{E}[\boldsymbol{SS}^{\boldsymbol{H}}]\boldsymbol{A}^{\boldsymbol{H}} + \mathbb{E}[\boldsymbol{nn}^{\boldsymbol{H}}]$$

$$= \boldsymbol{AR_{SS}A}^{\boldsymbol{H}} + \boldsymbol{\sigma}^{\mathbf{2}}\boldsymbol{I_{M\times M}} \quad (\mathbf{4.12})$$

Where,

$\mathbb{E}$ is the statistical expectation,

$\boldsymbol{\sigma}^{\mathbf{2}}$ is the variance of the noise,

$(\,)^{H}$ is conjugate transpose (Hermitian),

and $\boldsymbol{I_{M\times M}}$ is identity matrix.

Eq 4.11 is computationally challenging to calculate in practice since only a small number of data sets are collected for the processing. As a result, an approximated (i.e., estimated) version of $\boldsymbol{R_{XX}}$ is effectively calculated as a temporal average of a limited number of snapshots. as shown in **Eq 4.13** [29][34]:

$$\widehat{\boldsymbol{R}} = \frac{\mathbf{1}}{\mathbf{N}} \sum_{\boldsymbol{n=0}}^{\mathbf{N-1}} \mathbf{X}\mathbf{X}^{\mathbf{H}} \quad (\mathbf{4.13})$$

Where,

$\mathbf{N}$ is the number of snapshots (Samples).

4.1.3 Singular Value Decomposition (SVD)

SVD is an efficient and robust method for factorizing the matrix into three matrices. SVD is used as a technique for splitting the data matrix's range space into two complementary subspaces.

The SVD of an $m \times n$ complex matrix $\mathbf{X}$ is expressed as shown below:

$$\mathbf{X} = \boldsymbol{U}\,\boldsymbol{\Sigma}\,\boldsymbol{V}^{\boldsymbol{H}} \quad (\mathbf{4.14})$$

Where $\boldsymbol{U}$ is a complex unitary matrix with a size of $(\boldsymbol{m} \times \boldsymbol{m})$,

$\boldsymbol{\Sigma}$ is a rectangular matrix with the size of ($\boldsymbol{m} \times \boldsymbol{n}$),

and $\boldsymbol{V}$ is an $\boldsymbol{n} \times \boldsymbol{n}$ complex unitary matrix.

$\boldsymbol{\Sigma}$ has non-negative real values on the diagonal.

The matrices $\boldsymbol{U}$ and $\boldsymbol{V}$ are real orthogonal matrices when $\mathbf{X}$ is real. The values $\boldsymbol{\Sigma_i}$ of the diagonal of $\boldsymbol{\Sigma}$ are known as the singular values of $\mathbf{X}$**.**The rank of $\mathbf{X}$ is equal to the number of nonzeros of those singular entries. The columns of $\boldsymbol{U}$ and the columns of $\boldsymbol{V}$ are named as the left-singular and right-singular vectors of $\mathbf{X}$, respectively.

For our covariance matrix (i.e., $\mathbf{X}\mathbf{X}^{\mathbf{H}}$) :

$$\mathbf{X}\mathbf{X}^{\mathbf{H}} = \boldsymbol{R}_{\mathbf{XX}} = \boldsymbol{U}\,\boldsymbol{\Sigma}\,\boldsymbol{V}^{\boldsymbol{H}}\,\boldsymbol{V}\,\boldsymbol{\Sigma}\,\boldsymbol{U}^{\boldsymbol{H}} = \boldsymbol{U}\boldsymbol{\Sigma}\boldsymbol{U}^{\boldsymbol{H}}$$

Where $\boldsymbol{R}_{\mathbf{XX}}$ is $M \times K$ matrix, $\boldsymbol{U}$ is $M \times M$, and $\boldsymbol{V}$ is $K \times K$

Here, $\boldsymbol{M}$ is the number of antennas, and $\boldsymbol{K}$ is the number of the signals and $\boldsymbol{\Sigma}$ are $M \times K$ and contains the singular values in descending order:

$$\boldsymbol{\sigma_{s1}} \geq \boldsymbol{\sigma_{s2}} \geq \boldsymbol{\sigma_{s3}} \ldots\ldots\ldots \boldsymbol{\sigma_{sK}} \geq \mathbf{0}$$

In our assumed data model, matrix $\boldsymbol{A}$ is a Vandermond matrix, and columns are independent. Thus, if $\boldsymbol{R}_{ss}$ is a nonsingular matrix which means its rank is equal to the number of signals $\boldsymbol{(K)}$**,** then:

$$\boldsymbol{Rank}(\boldsymbol{A}\boldsymbol{R}_{\boldsymbol{SS}}\boldsymbol{A}^{\boldsymbol{H}}) = \boldsymbol{K}$$

It is worth mentioning here is that $\boldsymbol{R}_{\mathbf{XX}}$ Has real eigenvalues (i.e., Hermitian). It has positive eigenvalues ($\boldsymbol{K}$) and zero eigenvalues ($\boldsymbol{M} - \boldsymbol{K}$).

Now with the case of noise:

$$\boldsymbol{R}_{\mathbf{XX}} = \boldsymbol{A}\boldsymbol{R}_{\boldsymbol{S}}\boldsymbol{A}^{\boldsymbol{H}} + \boldsymbol{\sigma}^{\mathbf{2}}\boldsymbol{I}_{\boldsymbol{m}\times\boldsymbol{m}}$$

- σ^2>0, $\boldsymbol{R}_{\mathbf{XX}}$ is a full rank matrix.
- There are $\boldsymbol{M}$ positives eigenvalues (real) sorted as $\sigma_{s1} \geq \sigma_{s2} \geq \sigma_{s3} \ldots\ldots,, \sigma_{sM} \geq 0$
- These eigenvalues relate to $\boldsymbol{M}$ eigenvectors ($v_1, v_2 \ldots\ldots, v_M$).
- The eigenvectors are orthogonal because $\boldsymbol{R}_{\mathbf{XX}}$ is Hermitian.
- For the signals, there are $\boldsymbol{K}$ eigenvalues and $\boldsymbol{K}$ corresponding eigenvectors.
- The eigenvalues are resulted by the summation of the matrix AR_sA^H and σ^2.
- This means there are ($\boldsymbol{K}$) eigenvalues that correspond to the signals.
- There are ($\boldsymbol{M} - \boldsymbol{K}$) eigenvalues that correspond to the noise.

According to what was stated so far, the EigenVectors matrix can be decomposed to:

- signal-subspace (corresponds to the eigenvectors of signals)
- Noise-subspace (corresponds to the eigenvectors of the noise).

Hence, the matrix of $\boldsymbol{U}$ can be divided as:

$$\boldsymbol{U} = [\boldsymbol{U_s}, \boldsymbol{U_n}] \qquad (\mathbf{4.15})$$

$\boldsymbol{U_s}$, is the $\boldsymbol{M}\times\boldsymbol{K}$ matrix contains the eigenvectors related to $\boldsymbol{K}$ most significant singular values (largest) and the matrix $\boldsymbol{U_n}$ Contains the eigenvectors of the $\boldsymbol{M}-\boldsymbol{K}$ smallest eigenvalues.

The range space of $\boldsymbol{U_s}$ equals the space spanned by the signal (i.e., related to the steering vectors)[35]

$\boldsymbol{U_s}$ is referred to as "signal subspace." while $\boldsymbol{U_n}$ is the "noise subspace."

Because $\boldsymbol{U}$ is a "unitary matrix," the two subspaces are orthogonal, so that [28]

$$\boldsymbol{U_s^H U_n = 0}$$
$$\boldsymbol{a^H(\theta) U_n = 0}$$

Finally, the eigendecomposition of $\boldsymbol{R_{XX}}$ can be written as:

$$\boldsymbol{R_{XX} = U\Sigma U^H = [U_s\ U_n] \begin{bmatrix} D_s & 0 \\ 0 & \sigma^2 I \end{bmatrix} [U_s\ U_n]^H} \qquad (\mathbf{4.16})$$

The following sum up the previous procedures.

- The matrix U is split into two matrices, U_s with a size of ($\boldsymbol{M \times K}$), and $\boldsymbol{U_n}$ with a size of ($\boldsymbol{M \times [M - K]}$)
- The columns of ($\boldsymbol{U_s}$) are composed of the $\boldsymbol{K}$ eigenvectors represent the signals.
- The columns of ($\boldsymbol{U_n}$) are composed of $\boldsymbol{M - K}$ eigenvectors represent the noise.
- Matrix $\boldsymbol{D}$ contains in its diagonal the eigenvalues of the covariance matrix $\boldsymbol{R_{XX}}$.
- $\boldsymbol{D}$ is split into two diagonal matrices.
- $\boldsymbol{D_s}$ with the size of ($\boldsymbol{K \times K}$) for the signal eigenvalues.
- $\sigma^2 I$ is ($\boldsymbol{M - K}$) × ($\boldsymbol{M - K}$) has the noise eigenvalues in its diagonal which is $\boldsymbol{M - K}$

4.2 Estimation methods

The problem of direction-finding has been extensively researched, and many techniques for estimating the Angle (AoA) and other approaches that depend on the structure or geometry of the antenna system are available. This section will review several algorithms by emphasizing their mathematical model and complexity. Additionally, a literature review of new techniques will be presented.

The Angle of Arrival estimate methods may be divided into spatial spectrum-based and parametric. The spatial spectrum-based approach produces a spectral function and detects its peaks. These algorithms have lower complexity than parametric algorithms; however, they do not always provide adequate precision. In terms of accuracy, parametric algorithms surpass the spectral-based approach; nevertheless, the computational cost is high. The pursuit of low complexity in the network subsystems is always one of the criteria for cellular networks; therefore, the parametric method will be beyond the scope of the thesis.

The methods also can be categorized and grouped according to the mathematical model. Conventional beamforming, MVDR, and Linear prediction are considered within Beamforming techniques. MUSIC, minimum-norm, ESPRIT, Root-MUSCI, and U-ESPRIT are Sub-space methods.

For the Uniform Linear Array Model **Eq. 3.1** of the signal $\boldsymbol{y(n)}$ can be represented in a vector form as follows [34]:

$$\boldsymbol{y(n) = W^H X(n)} \qquad (\mathbf{4,17})$$

Where,

$\boldsymbol{W}$ is the beamforming weight vector,

and $\mathbf{X} = \boldsymbol{AS(n)} + \boldsymbol{n(n)}$ is the received data by the array antenna.

4.2.1 Conventional Beamforming (Bartlett)

In the conventional beamforming approach, the weight vector in **Eq. 4.17** is equivalent to the steering vector (i.e., $W = a(\theta)$). $\boldsymbol{\theta}$ is the searching angle.

This method calculates the Angle of Arrival by finding the spectral of the signal's strength with respect to the angles, then the correspondent angles of the peaks represent the Angle of Arrival of the signals.

Practically, $\boldsymbol{W} = \boldsymbol{a}(\theta)$ is normalized as follows:

$$\boldsymbol{W_{Bart}} = \frac{\boldsymbol{a}(\boldsymbol{\theta})}{\sqrt{\boldsymbol{a^H}(\boldsymbol{\theta})\boldsymbol{a}(\boldsymbol{\theta})}} \qquad (\mathbf{4.18})$$

The basic working principle is that the weight vector is like a spatial filter; it produces a peak when it matches the impinging signals with the Angle of Arrival. After applying **Eq. 4.18** in **Eq. 4.17**, the power function which represents the spatial spectrum is given by:

$$\boldsymbol{P_{Bart}}(\boldsymbol{\theta}) = \frac{\boldsymbol{a^H}(\boldsymbol{\theta})\, \boldsymbol{R_{XX}}\, \boldsymbol{a}(\boldsymbol{\theta})}{\boldsymbol{a^H}(\boldsymbol{\theta})\boldsymbol{a}(\boldsymbol{\theta})} \qquad (\mathbf{4.19})$$

Although this method is categorized as simple and low complexity, its accuracy degrades when many incoming signals are present. The traditional Beamformer directs the strongest beam in a certain direction, indicating the arrival direction with the peak power. This implies that, due to the interference signals, the spatial spectrum's peaks may be shifted away from the actual AoA. This implies that when signals are closely spaced, the algorithm is unable to differentiate them. Therefore, traditional beamforming works well when just a few incoming signals; otherwise, performance degrades.

Using additional antenna elements improves the algorithm's resolution; nevertheless, this raises the algorithm's complexity.

The major steps of the algorithm are summarized below in Table 4.1.

Table 4.1: Conventional Beamformer AoA Estimation Algorithm.

Algorithm 1: Conventional Beamformer AoA
1. Compute the covariance matrix $\widehat{R}$ in Eq. 4.13
2. Find the Spatial Spectrum over a scanning angular range in Eq. 4.19
3. Find the highest K Peaks.

4.2.2 MVDR

Capon's Minimum Variance Distortion Less (MVDR), developed in 1967[36] attempts to address the shortcomings of the standard Beamformer. To shape the beam in the wanted direction, the traditional Beamformer employs all degrees of freedom. As previously mentioned, it has a poor resolution, especially when there are a large number of incoming signals. The MVDR concept for dealing with this issue is to use certain degrees of freedom to create a beam in the look direction and minimizes the other directions to obliterate all other signals.

To do this, a restricted minimization problem must be addressed. It can be achieved by limiting the beamformer gain to "1" in the wanted direction (main loop) and using the remaining DOF (degrees of freedom) to reduce the other side loops. It can be represented mathematically as:

$$\min_{W} \ (W^H R_{XX} W) \quad subject\ to \quad (W^H a(\theta) = 1) \tag{4.20}$$

By retaining the gain in the look direction, the trivial Solution is avoided for $W = 0$ (i.e., no signal will be formed).

This technique is often referred to as the minimal variance distortionless response (MVDR) because of that reduction of the power (i.e., variance) of the other signal components or side loops while conveying the appropriate signal in the wanted direction without distortion. The following equation gives the weight vector:

$$W_{Cap} = \frac{R_{XX}^{-1} a(\theta)}{a^H(\theta) R_{XX}^{-1} a(\theta)} \tag{4.21}$$

The following equation gives the spatial spectrum in this method:

$$P_{MVDR}(\theta) = \frac{1}{a^H(\theta) R_{XX}^{-1} a(\theta)} \tag{4.22}$$

Even though Capon's method improves the accuracy, especially in closed-spaced sources, the resolution is still insufficient and is considered a low-resolution algorithm if the correlated signals are present[37]. The reason for that comes from the fact that the covariance matrix becomes singular for the correlated signals leading to a destructive combination of the correlated component when the output power is minimized. Moreover, MVDR requires more computational complexity than the conventional Beamformer, intuitively because of the computation of the inverse covariance matrix in **Eq. 4.22**. The steps of the algorithm are given below in **Table 4.2**:

Table 4.2: MVDR AoA Estimation Algorithm.

Algorithm 2: MVDR AoA
1. **Compute the covariance matrix $\widehat{R}$ in Eq. 4.13**
2. **Compute the inverse of $\widehat{R}$.**
3. **Find the spatial spectrum over the scanning angular region using Eq. 4.22**
4. **Find the K highest Peaks**

4.2.3 MUSIC

Multiple Signals Classification Algorithm is sometimes referred to as super-resolution algorithm. It is based on the principle of orthogonal subspaces, where the algorithm decomposes the covariance matrix to create a signal subspace orthogonal to the noise subspace. As demonstrated in **section 4.1.3**, the steering vectors are related to the incoming signals, which represent the signal subspace; Meaning that there is orthogonality between the steering vectors and the noise subspace. Scanning over all sets of steering vectors to find orthogonal ones to the noise subspace is the premise of the MUSIC algorithm to solve the problem of AoA. The cost function in MUSIC is $a^H(\theta) U_n$ and if and only if when the steering vector corresponds to the incoming signal, the cost function will be zero. [34]

$$a^H(\theta) U_n = 0 \tag{4.23}$$

Where $\boldsymbol{U_n}$ is the noise subspace matrix. The spatial spectrum function of this method is shown below:

$$\boldsymbol{P_{MUSIC}(\theta) = \frac{1}{a^H(\theta) U_n U_n^H a(\theta)}} \quad (4.24)$$

This technique of finding AoA is summarized below Table:

Table 4.3: MUSIC AoA Estimation Algorithm.

Algorithm3: MUSIC AoA
1. Compute the covariance matrix $\widehat{R}$ in Eq. 4.13
2. Perform Eigen Decomposition by using Eq. 4.16
3. Finding the spatial spectrum as in Eq. 4.24
4. Find the K highest Peaks

Apart from the fact that MUSIC is a high-resolution AoA algorithm that surpasses the preceding two techniques, the following remarks should be noted while employing this algorithm:

- MUSIC method is a search-based algorithm that is complex and complex in terms of computation; the situation will be worst in some applications, e.g., joint azimuth and elevation estimation.[38]
- Theoretically, MUSIC achieves an arbitrarily high resolution. However, it is limited to uncorrelated signals; however, performance degrades in the presence of correlated signals [39].
- The method assumes that the incoming signals are fewer than the antenna elements, which implies that it can differentiate up to $\boldsymbol{M-1}$ signals, where M is the number of antenna elements, which results in a singular covariance matrix.
- Practically speaking, MUSIC assumes there is orthogonality between the two subspaces (steering vector and the noise subspace), but this is not guaranteed due to the estimation error for the $\boldsymbol{U_n}$. [34]

4.2.4 ESPRIT

ESPRIT which stands for "Estimation of Signal Parameters via Rotational Invariance Technique" is one of the subspace methods used for AoA measurement. The ESPRIT technique for AoA finding was originally introduced by (Roy and Kailath)[40]. The major distinction between the MUSIC and ESPRIT algorithms is that the former uses the noise subspace, whereas the latter employs the signal subspace in combination with a rotating variance method. Using ESPRIT for Angle of Arrival estimation means there is no need to optimize or search any spectral measure, which means that using the ESPRIT algorithm reduces the computational complexity in comparison with the MUSIC method, which requires scanning over large ranges of angles. The concept of working in ESPRIT is to divide the array antenna of $\boldsymbol{M}$ elements into two subarrays. These subarrays can be overlapped (i.e., some elements might belong to both subarrays), as shown in **Figure 4.2**. Different distributions of the antenna elements can be used when dividing the subarrays, and some of them are non-uniform while the most common one is the uniform, as shown in **Figure 4.2**.

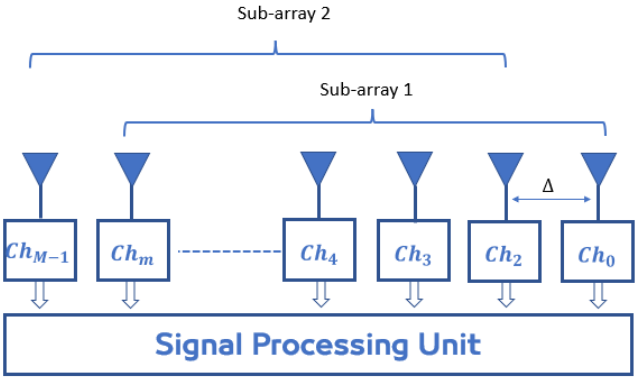

Figure 4.2: Two Sub-arrays for ESPRIT Algorithm

The output of the two subarrays can be expressed as below: [41]

$$\mathbf{X_1}(\boldsymbol{n}) = \sum_{\boldsymbol{k=0}}^{\boldsymbol{K-1}} \boldsymbol{S_k}(\boldsymbol{n})\boldsymbol{a}(\boldsymbol{\theta_k}) + \boldsymbol{n_{X1}}(\boldsymbol{n}) \tag{4.29}$$

$$\mathbf{X_2}(\boldsymbol{n}) = \sum_{\boldsymbol{k=0}}^{\boldsymbol{K-1}} \boldsymbol{S_k}(\boldsymbol{n})\boldsymbol{e}^{\frac{-j2\pi\Delta\sin(\theta_k)}{\lambda}}\boldsymbol{a}(\boldsymbol{\theta_k}) + \boldsymbol{n_{X2}}(\boldsymbol{n}) \tag{4.30}$$

Then in a matrix form:

$$\mathbf{X_1} = \boldsymbol{AS} + \boldsymbol{n_{X1}} \tag{4.31}$$

$$\mathbf{X_2} = \boldsymbol{A\Phi S} + \boldsymbol{n_{X2}} \tag{4.32}$$

Where $\boldsymbol{\Phi}$ is a diagonal matrix:

$$\boldsymbol{\Phi} = \boldsymbol{diag}\left\{\boldsymbol{e}^{-\frac{\boldsymbol{j2\pi}}{\boldsymbol{\lambda}}\boldsymbol{\Delta}\sin(\boldsymbol{\theta_0})}, \ldots, \boldsymbol{e}^{\frac{\boldsymbol{-j2\pi}}{\boldsymbol{\lambda}}\boldsymbol{\Delta}\sin(\boldsymbol{\theta_{K-1}})}\right\} \tag{4.33}$$

$\boldsymbol{\Phi}$ with a size of $(K \times K)$ connects the output of the two subarrays, denoted by the "Rotational Operator," and indicates an additional delay induced by $\boldsymbol{\Delta}$ on the second subarray.

$$\mathbf{X}(\boldsymbol{n}) = \begin{bmatrix}\mathbf{X_1}(\boldsymbol{n})\\ \mathbf{X_2}(\boldsymbol{n})\end{bmatrix} = \begin{bmatrix}\boldsymbol{A}\\ \boldsymbol{A\Phi}\end{bmatrix}\boldsymbol{S}(\boldsymbol{n}) + \begin{bmatrix}\boldsymbol{n_1}(\boldsymbol{n})\\ \boldsymbol{n_2}(\boldsymbol{n})\end{bmatrix} = \boldsymbol{Q_s S}(\boldsymbol{n}) + \boldsymbol{n}(\boldsymbol{n}) \tag{4.34}$$

Using the ESPRIT algorithm, the Estimation of Angle of Arrival requires two steps [23], first by computing the signal subspace and then measuring the $\boldsymbol{\Phi}$ operator.

Estimating the signal subspace relies on the $\boldsymbol{Qs}$ structure. Without knowing $\boldsymbol{A}$, the diagonal elements of $\boldsymbol{\Phi}$ can be estimated by using the structure of $\boldsymbol{Qs}$. The $\boldsymbol{Qs}$ columns span the signal subspace of the combined subarrays.

As a result, the eigen decomposition of $\boldsymbol{R_{XX}}$ Yields $\boldsymbol{Q} = [\boldsymbol{Qs}\ \boldsymbol{Qn}]$.

$\boldsymbol{Qs}$ and $\boldsymbol{E_S}$ are linked by a $\boldsymbol{K} \times \boldsymbol{K}$ transformation $\boldsymbol{T}$ if $\boldsymbol{E_S}$ is a matrix with columns that provide the basis for the signal subspace relating to $\mathbf{X}$.

$$\boldsymbol{E_s} = \boldsymbol{Q_s}\,\boldsymbol{T} = \begin{bmatrix}\boldsymbol{AT}\\ \boldsymbol{A\Phi T}\end{bmatrix} = \begin{bmatrix}\boldsymbol{E1}\\ \boldsymbol{E2}\end{bmatrix} \tag{4.35}$$

Where the range of $\boldsymbol{E_1}$ equal to the range of both $\boldsymbol{E_2}$, and $\boldsymbol{A}$ [40], it is possible to define a nonsingular $\boldsymbol{K} \times \boldsymbol{K}$ matrix $\boldsymbol{\Psi}$ as follows:

$$\boldsymbol{E_1\Psi} = \boldsymbol{E_2} \tag{4.36}$$

and $\boldsymbol{\Psi}$ is expressed as:

$$\boldsymbol{AT\Psi} = \boldsymbol{A\Phi T} \tag{4.37}$$

$$\boldsymbol{AT\Psi T^{-1} = A\Phi} \quad (\mathbf{4.38})$$

$$\boldsymbol{\Psi = T^{-1}\Phi\, T} \quad (\mathbf{4.39})$$

Consequently:

- The eigenvalues of $\boldsymbol{\Psi}$ should be equivalent to the diagonal entries of $\boldsymbol{\Phi}$.
- The eigenvectors of $\boldsymbol{\Psi}$ must be $\boldsymbol{T}$ columns.

This is the critical relationship that shaped ESPRIT and its characteristics.

The signal parameters are deduced as nonlinear functions of the singular values of the operator that converts $(\boldsymbol{E_1})$ spanning an m-dimensional signal subspace to $(\boldsymbol{E_2})$[40].

The next step is to get an estimate of the rotating subspace $\boldsymbol{\Psi}$. As a result, the processed data is influenced by noise. **Eq. 4.36** will not be precisely solved since $\boldsymbol{E_1}$ and $\boldsymbol{E_2}$ do not span the same subspace exactly. There are two ways to get an accurate find the rotating subspace $\boldsymbol{\Psi}$,

First is the Least-squares estimation method (LS), and second by the Total Least Squares estimation method (TLS).

As a result of the aforementioned techniques, there exist two versions of ESPRIT. Least squares and total least squares.

Consider the matrix model $\boldsymbol{AX = B}$, which is analogous to the problem we are attempting to solve. The least-square approach presupposes that Matrix A is given, and all errors are due by noise, and the Least Square Solution may be stated as:

$$\boldsymbol{\widehat{X} = [AA^H]^{-1}\, A^H B} \quad (\mathbf{4.40})$$

Where $\boldsymbol{\widehat{X}}$ is the estimate of $\boldsymbol{X}$.

It is worth noting that the least square technique does not consider that $\boldsymbol{A}$ computed from the received data, which most likely contains noise. Total least-square consider this issue. Total Least square is out of the scope of this section.

To conclude, for the purposes of conventional ESPRIT, the array antenna in **Figure 4.2** has a complete overlap (i.e., each sub-array contains $\boldsymbol{M-1}$ elements). $\boldsymbol{J_1}$, which includes the beginning $(\boldsymbol{M-1})$ rows of $\boldsymbol{A}$, while $\boldsymbol{J_2}$, contains the last $(\boldsymbol{M-1})$ rows, can be used to construct the selection matrices. This could be written as:

$$\boldsymbol{J_1 = [I_{M-1}\ 0] \in R^{M-1\times M}} \textbf{ and } \boldsymbol{J_2 = [0\ I_{M-1}] \in R^{M-1\times M}}$$

where $\boldsymbol{I_{M-1}}$is an identity matrix.

The shift-invariance property of the steering matrix containing the steering vectors can be expressed as a matrix as:

$$\boldsymbol{J_1 A\Phi = J_2 A} \quad (\mathbf{4.41})$$

Without taking into account noise, $\boldsymbol{R_{XX}}$ SVD is expressed as:

$$\boldsymbol{R_{XX} = AR_{SS}A^H = \ U_{SS}\Sigma_K U_{SS}^H} \quad (\mathbf{4.42})$$

According to **Eq. 4.42**, the columns in matrix $\boldsymbol{A}$ span the signal subspace, so:

$$\boldsymbol{S = Range\,\{A\} = Range\{U_s\}} \quad (\mathbf{4.43})$$

Therefore, there is a nonsingular $\boldsymbol{T_A}$ in a size of $(\boldsymbol{K\times K})$ gives $\boldsymbol{A = U_s T_A}$. The singular vectors of $\boldsymbol{U_s}$, which span the signal subspace, may therefore be used to describe the shift-invariance property:

$$\boldsymbol{J_1 U_s T_A \Phi = J_2 U_s T_A \iff J_1 U_s \Psi = J_2 U_s} \quad (\mathbf{4.44})$$

Where $\boldsymbol{\Psi} = \boldsymbol{T}A\Phi\boldsymbol{T}_A^{-1}$ Is the rotating operator, which is nonsingular with a size of ($\boldsymbol{K} \times \boldsymbol{K}$) signal subspace. consequence, $\boldsymbol{\Psi}$, and its singular values which include Angle of Arrival information can be obtained by estimating the signal subspace $\mathbf{U}_S$

$$\boldsymbol{J_1 U_s \Psi} \approx \boldsymbol{J_2 U_s} \quad (\mathbf{4.45})$$

This method may not provide a precise solution. Furthermore, the size of the subarrays $\boldsymbol{M - 1}$ must be more than or equal to the incoming signals $\boldsymbol{K}$ to find all the Angles of Arrivals. As previously stated $\boldsymbol{\Psi}$ can be calculated by solving the preceding equation using either Least Square or Total Least Square. For the Least Square case:

$$\widehat{\boldsymbol{\Psi}} = [\boldsymbol{J_1 U_s}(\boldsymbol{J_1 U_s})^{\boldsymbol{H}}]^{-1} (\boldsymbol{J_1 U_s})^{\boldsymbol{H}} \boldsymbol{J_2 U_s} \quad (\mathbf{4.46})$$

Finally, $\boldsymbol{J}_1$ and $\boldsymbol{J}_2$ are known. Then, since the $\boldsymbol{K}$ eigenvalues $\boldsymbol{\phi_k}$ of $\boldsymbol{\Psi}$ are estimated, AoAs can be estimated as follows:

$$\boldsymbol{\Psi} = \boldsymbol{T}^{-1}\boldsymbol{\Psi T}$$

$$\boldsymbol{\theta_k} = \mathbf{arcsin}\left(\frac{-\boldsymbol{\lambda}\,.\,\boldsymbol{arg}(\boldsymbol{\phi_k})}{\mathbf{2}\boldsymbol{\pi\Delta}}\right) \quad (\mathbf{4.47})$$

$$\boldsymbol{\phi_k} = \boldsymbol{e}^{\frac{-j2\pi}{\lambda}\boldsymbol{\Delta sin}(\boldsymbol{\theta_k})} \quad \boldsymbol{k} = \mathbf{1, 2, \ldots\ldots K} \quad (\mathbf{4.48})$$

The ESPRIT algorithm differs from the previously mentioned methods in this section in that the prior algorithms require a computationally costly comprehensive search over all angles to find peaks in the spatial spectrum. The main steps of the ESPRIT algorithm are given in the following table:

Table 4.4: ESPRIT AoA estimation algorithm

Algorithm 4: ESPRIT AoA
1. Compute the covariance matrix $\widehat{\boldsymbol{R}}$ in Eq. 4.13
2. Perform EVD as in Eq. 4.16
3. Solve Eq. 4.46 to find $\widehat{\boldsymbol{\Psi}}$
4. Find eigenvalues of $\widehat{\boldsymbol{\Psi}}$
5. Find the angles using Eq. 4.47

4.2.5 Root-MUSIC

Many attempts were made to improve the MUSIC algorithm, which is an excellent resolution algorithm. The majority of the updated versions of MUSIC attempt to enhance MUSIC's accuracy and/or decrease the computing cost of the method. Root-MUSIC is one of the MUSIC variants that attempts to reduce computational complexity while improving the resolution[42] The concept of Root-MUSIC is to find the roots of a polynomial of the denominator of MUSIC spatial spectrum.

$$\boldsymbol{J(z)} = \boldsymbol{a^H(\theta) U_n U_n^H a(\theta)} \quad (\mathbf{4.49})$$

Now the steering vector of the ULA can be expressed as follows:

$$\boldsymbol{a(z)} = [\mathbf{1}\ \boldsymbol{z}\ \boldsymbol{z^2}\ \ldots\ \boldsymbol{z^{M-1}}]^{\boldsymbol{T}} \quad (\mathbf{4.50})$$

Where $\boldsymbol{z}$ for is expressed as:

$$z = e^{-\frac{j2\pi}{\lambda} m\Delta \sin(\theta)} \quad (4.51)$$

The Angle of Arrival information for the signal is given within the roots of $J(z)$. The roots are located within a unit circle. The positions of the roots may vary from the circle due to the presence of noise. In this situation, the roots nearest to that circle represent the signal component.[43]

The angles can be found by using the following equation:

$$\theta_k = \arcsin\left[-\frac{\lambda}{2\pi\Delta} arg(z_k)\right], \quad for\ k = 1, 2, \ldots . K \quad (4.52)$$

The algorithm steps are given in the below Table:

Table 4.5: R-MUSIC AoA estimation algorithm

Algorithm 5: R-MUSIC AoA
6. Compute the covariance matrix $\widehat{R}$ in Eq. 4.13
7. Perform EVD as in Eq. 4.16
8. Compute $U_n U_n^H$
9. Find the roots of J(z) in Eq. 4.49
10. Find the angles using Eq. 4.52

4.2.6 Minimum Norm

The minimum norm technique is suitable for linear arrays and may be viewed as an enhanced version of MUSIC for estimating AoA. The expression of the spatial spectrum that is used to identifies the peaks is given below [37] :

$$P_{MinNorm}(\theta) = \frac{1}{|a^H(\theta) U_n U_n^H e e^H U_n U_n^H a(\theta)|} \quad (4.53)$$

Where, U_n is the noise subspace

e is equaled to the first column of identity matrix of size $M \times M$.

The Minimum Norm algorithm gives a better resolution than the MUSIC algorithm, at least when it is used in the uniform linear array [44]. The major steps of the algorithm are shown in Table (4.6)

Table 4.6: Min. Norm AoA Estimation Algorithm.

Algorithm 6: Min. Norm AoA
1. Compute the covariance matrix $\widehat{R}$ in Eq. 4.13
2. Perform EVD as in Eq. 4.16
3. Use Eq.4.53 to compute the spatial spectrum.
4. Find the Highest K peaks.

4.2.7 DFT based AoA

Most of the previously mentioned methods rely heavily on the estimated version of the covariance matrix and require many snapshots to obtain higher accuracy and resolution. The angle of Arrival based on DFT may give a solution for applications requiring AoAs by

only a few snapshots. DFT method can be used to estimate AoA with just one snapshot. However, the DFT algorithm's precision pales in contrast to high-resolution techniques like MUSIC. Larger antennas element can boost the performance of DFT, for example with the accessible massive antennas in 5G NR and beyond. DFT AoA has an extremely low computational complexity that does not grow with the number of antenna components.

The proposed approach in [45] employs Discrete Fourier Transform (DFT) for AoA finding. It was assumed that the environment is noise-free to achieve high accuracy in the Estimation with few antenna elements. However, as mentioned earlier, this problem might be solved with 5G NR and beyond as there will be a massive number of antennas.

By applying $\boldsymbol{N}$-points of DFT (zero-padding of $\boldsymbol{N-M}$) to the input signal:

$$\boldsymbol{x_m(n) = s_k(n) e^{-\frac{j2\pi}{\lambda} m\Delta \sin(\theta)}}$$

$$\boldsymbol{X(p) = \sum_{i=0}^{N-1} x_i(n) e^{-\frac{j2\pi ip}{N}} = \sum_{i=0}^{N-1} \left(\sum_{k=1}^{K} s_k(n)\, e^{-\frac{j2\pi}{\lambda} i\Delta \sin(\theta_k)} \right) e^{-\frac{j2\pi}{N} ip} + \sum_{i=0}^{N-1} n_i(\mathrm{n})\, e^{-\frac{j2\pi}{N} ip}}$$

$$\boldsymbol{= \sum_{k=1}^{K} s_k(n) \left(\sum_{i=0}^{N-1} e^{-j\left(\frac{2\pi}{\lambda}\Delta \sin(\theta_k) + \frac{2\pi}{N} p\right) i} \right) + \sum_{i=0}^{M-1} n_i(\mathrm{n})\, e^{-\frac{j2\pi}{N} ip}}, \qquad \boldsymbol{(4.54)}$$

for, $0 \le p \le N-1$

$$\boldsymbol{X(p) = \sum_{k=1}^{K} s_k(\mathrm{n}) \frac{sin\left(N\frac{2\pi}{\lambda}\Delta \sin(\theta_k)}{2} + \pi p \right)}{sin\left(\frac{2\pi}{\lambda}\Delta \sin(\theta_k)}{2} + \frac{\pi p}{N} \right)} e^{-j\left(\frac{2\pi}{\lambda}\Delta \sin(\theta_k) + \frac{2\pi p}{N}\right)\left(\frac{N-1}{2}\right)} + \sum_{i=0}^{M-1} n_i(\mathrm{n})\, e^{-\frac{j2\pi}{N} ip} \quad (4.55)$$

$\boldsymbol{X(p)}$ is the DFT of the input signal for the nth snapshot. The $\boldsymbol{K}$ largest peaks of $\boldsymbol{X(p)}$ would occur at, $\boldsymbol{p = \frac{\left(-N\frac{j2\pi}{\lambda}\Delta \sin(\theta_k)\right)}{2\pi}}$, $\boldsymbol{for\ k = 1, 2, \ldots . K}$

or equivalent at:

$$\boldsymbol{\theta_k = \arcsin\left(-\frac{2p}{N}\right)} \qquad \boldsymbol{(4.56)}$$

$$\boldsymbol{for, k = 1, 2, \ldots . , K}$$

This thesis modified this method to take $\mathbf{N}$ snapshots, then averaging the spatial spectrum before finding the peaks to enhance the accuracy. For the Fast realization of this method, Fast Fourier Transform was used to implement DFT-Based AoA. The steps of this technique are given in below Table:

Table 4.7: FFT AoA Estimation Algorithm.

Algorithm 7: FFT AoA
1. **Compute FFT for X** 2. **Find AoAs using Eq. 4.56** 3. **Find the K highest Peaks by plotting the FFT spectrum with respect to step 2**

4.2.8 CASCADE AoA

From the previous illustrated measurement methods, it can be noticed that there is a tradeoff between accuracy and complexity, which is the challenge in the AoA problem. In 5G systems and beyond, it is necessary to design an algorithm that meets positioning use cases that reach the level of centimeters of accuracy in some indoor scenarios. At the same time, the measurement time should be short enough to prevent any delay in the positioning algorithm.

MUSIC algorithm is a high-resolution algorithm that many researchers are still trying to modify by reducing its complexity in terms of the time-consuming.

In [46], a CASCADE method with a flexible massive array antenna was proposed to estimate AoA accurately and with low complexity. The proposed algorithm consists of two stages: first, using MVDR with a small-sized array antenna to find the ranges or groups of AoAs, then the second step employs beamspace MUSIC with the total array elements to estimate the fine resolution of AoAs. However, the mentioned method uses MVDR as the first stage, which has an apparent complexity and requires a high number of snapshots to estimate AoA correctly. Instead, this section proposes a simple, efficient, and fast algorithm based on combining the Fast method, which is FFT, and one of the most accurate methods, MUSIC. This combination constructs a CASCADE system, starts by fast-coarse estimation using the FFT method to indicate the range of the AoAs, then the second stage is scanning over that range using MUSIC algorithm. This CASCADE approach offers as high accuracy as MUSIC and reduces the time consuming of the MUSIC algorithm at the same time.

The range of the AoAs is determined by finding the angles that correspond to the minimum and maximum $\boldsymbol{K}$ peaks; then, an angle margin should be added to ensure that the next stage estimates the angle correctly.

$$\boldsymbol{\theta_{range} = \theta_{minPeak} - \vartheta \ to\ \theta_{maxPeak} + \vartheta} \qquad (\mathbf{4.57})$$

Where,

$\boldsymbol{\vartheta}$ is the margin that ensures the accuracy in the estimation; it can be 10^o For instance. By increasing that margin, the angular scanning region in the MUSIC algorithm will expand; therefore, it is preferable to maintain a small value of $\boldsymbol{\vartheta}$ that achieves the required accuracy in the estimation without increasing the searching region. **Table 4.8** shows the CASCADE algorithm steps.

Table 4.8: CASCADE AoA Estimation Algorithm.

Algorithm 6: CASCADE AoA
1. Compute FFT for $\mathbf{X}$
2. Find AoAs using Eq. 4.56
3. Find the K highest Peaks by plotting the FFT spectrum with respect to step 2.
4. Find the range of θ using Eq. 4.57
5. Compute the covariance matrix $\widehat{R}$ in Eq. 4.13
6. perform Eigen Decomposition by using Eq.4.16
7. Find the spatial spectrum as in Eq. 4.24 and by using the range computed in step 4.
8. Find the K highest Peaks

It is worth mentioning that this method can be further optimized and modified to detect

only the line of sight (LOS). This means the searching in the second stage of the algorithm will be, for instance $\pm 10^{o}$ of the LOS that detected by FFT. This modification will lead to a considerable reduction in the time-consuming, as will be explained in **section 5**. Moreover, focusing only on estimating the LOS will give more robustness against the correlated multipath signals, which might reduce the accuracy of the estimation.

4.3 Other Techniques and Estimation factors

The angle of Arrival estimation, often known as direction-finding, remains a problem in wireless communication, and many academics are working to enhance estimates by improving current methods or inventing new ones. The estimated Angle of Arrival can be used directly for applications such as localization applications that use the angular information as in[47], or it can assist in joining-localization applications like in [26], where the author used joint angle-time approach for positioning estimation where sounding reference signal used for time delay estimation.

In [48], the author employed Angle of arrival estimation in the sub-6 GHz band to reduce the searching in beam training in mm-waves. It was used MUSIC/R-MUSIC algorithms to estimate AoA, and then the estimated angle was passed to the mm-wave part for beam training. The last stage of the proposed approach was to find the range by using Time-weighted return (TWR).

Recently many efforts were put into the use of multiple sub-array antennas. However, this method requires to solve the synchronization problem. In [49], the author presented a new algorithm for synchronizing time, frequency, and the phase for multiple sub-arrays antenna to increase the resolution of AoA estimation by increasing the antenna aperture. The author utilized a Joint maximum likelihood optimization to synchronize the time and the frequency while using a Least mean square and ML to achieve the phase coherency. The algorithm was succeeded in an indoor environment of an anechoic chamber and outdoor as well. The transmitted signal is DASH7 Protocol signals. They also showed that the new algorithm does not depend on a fixed structure of the augmented array element number, where they provided a simulation example using UCA with four sub-arrays and different element numbers for each sub-array. However, this algorithm's complexity increases with the increase of the total number of subarray antennas which might not be suitable for a cellular network as there will be a massive number of antennas (i.e., Massive MIMO).

ViSA (Virtual-Subarray) based scheme was used in [50] for the AoA measurement. The main idea of the scheme is to divide the analog arrays into two virtual subarrays and exploit the phase difference between one pair of measurements for Angle of Arrival. A different construction of the subarray has been shown, which gives different accuracy of estimation as shown in the below Table:

Table 4.9: Antenna Indexes of VSA for Different Q_k Values [42]

Value of Q	Antenna Indexes of Virtual subarray 1	Antenna Indexes of Virtual subarray 2
$Q = 1$	0,2,4,6,8,10,12,14	1,3,5,7,9,11,13,15
$Q = 2$	0, 1, 4, 5, 8,9,12, 13	2,3,6,7,10,11,14,15
$Q = 4$	0, 1, 2, 3, 8,9, 10, 11	4,5, 6, 7,12, 13, 14, 15
$Q = 8$	0,1,2,3,4,5,6,7	9,10,11,12,13,14,15

It is shown that constructing with a doubled value of $\boldsymbol{Q}$ may result in a 6 dB SNR improvement. Furthermore, they developed two techniques for integrating ViSA with sequential scanning and multi-resolution scanning for improved performance utilizing the maximum likelihood principle.

Another approach is by using a coprime array for enhancing the Estimation. It can achieve a narrow beam pattern due to the co-array domain's large degrees of freedom. In [51], the authors proposed the AoA Estimation method Based on Combined Unitary ESPRIT for Coprime MIMO Radar. The suggested approach estimates coupled but imprecise AoA using Unitary ESPRIT, which reduces the difficulty of identifying the peak or iterations, as is the case in traditional methods. Then, based on coprime-ness, the unique AoA estimate may be obtained by identifying the coinciding solutions from the transmit and receive arrays. The paper showed that this proposed algorithm could handle $\boldsymbol{min}(\boldsymbol{M}(\boldsymbol{N}-\mathbf{1}),\boldsymbol{N}(\boldsymbol{M}-\mathbf{1}))$ targets while the conventional methods like UR-MUSIC can handle only $(\boldsymbol{M}+\boldsymbol{N}-\mathbf{2})$ where $\boldsymbol{N}$ and $\boldsymbol{M}$ are the numbers of transmitting and receiving array elements, respectively. It also provides better resolution for DoA estimation.

The multi-mode antenna is another method that has been developed and studied only for communications, with no consideration given to its potential for positioning. A multi-mode antenna (MMA) may be used as an alternate method for estimating DoA. It has been used in [52] There are two methods to signal to process using MMAs: one based on AIT (Array Interpolating Technique) and one based on WM (Wave Modeling), both of which take into account the nonidealized characteristics of the antenna, such as mutual coupling. They demonstrated that WM outperforms AIT in the high SNR domain and that the polarization characteristics of the incoming wave can be calculated.

The angle of Arrival techniques is affected by various factors that may decrease performance and render it inappropriate for contemporary applications. The Estimation, for example, is impacted by the sparse complicated environment [53]. Furthermore, the majority of the algorithm is impacted by the increase of antennas (i.e., Massive MIMO). It increases computational complexity, despite the fact that increasing the antenna elements boosts the performance for the majority of algorithms. Moreover, the performance of AoA algorithms degrades in the multipath Scenario, which is a real-world situation in cellular networks. To be successful in practice, it should be an extension or modification of the conventional algorithm. Spatial smoothing, for example, may be used to solve the multipath issue [54]. The spatial smoothing method spatially decorrelates received signals, reducing array antenna degrees of freedom. The calculated Angles of Arrival are less in number than the array antenna components. Furthermore, these techniques may need a certain arrangement of array antenna components. One of the other variables that needed to be considered is the number of snapshots. When the other array parameters stay constant, more snapshots result in better estimation for super-resolution techniques[55]. However, the method becomes increasingly complicated as the number of snapshots increases. Other issues are related to the antenna element distribution design, such as mutual coupling and incorrect antenna array element positioning.

5. SIMULATION AND PERFORMANCE EVALUATION

This section presents the results of the simulation that was carried out to evaluate the performance of the Angle of Arrival algorithms concerning different parameters that impact the accuracy, resolution, and complexity of the algorithms. Six algorithms from section four have been implemented in MATLAB to achieve the best accuracy in a minimum processing time. The selected algorithms are Bartlet Beamforming in **section 4.2.1**, MVDR in **section 4.2.2**, ESPRIT in **section 4.2.4**, FFT in **section 4.2.7**, and finally, the proposed CASCADE algorithm in **section 4.2.8**.

The evaluation was based on a spatial spectrum and two metrics: Root Mean Square Error (RMSE) and Elapsed Time Metric (ELTM), focusing on the line-of-sight detection (LOS) by assuming that the strongest signal corresponds to the LOS.

It was assumed during the simulation that a single user (i.e., UE) sends an SRS signal over a multipath channel to the Base Station (i.e., gNB). The base station has a Uniform Linear Array (ULA) with an $\boldsymbol{M}$ number of array elements. Meaning that only azimuth angle will be estimated.

The SRS 5G NR signal was generated and used as the primary signal to test the algorithms to make the simulation more realistic since that SRS is the main signal for uplink direction positioning in 5G. Furthermore, as stated in section four, the multipath signals are correlated, which affects the performance of the majority of the algorithms. 5G toolbox in MATLAB 2021a was used to generate the baseband 5G NR uplink signal with a specific configuration of SRS symbols and for implementing all the algorithms mentioned earlier.

Section 5.1 presents the general simulation setup, SRS configuration, and generating 5G NR Uplink waveform. **Section 5.2** concerns the implementation of the algorithms. The simulation metrics used to assess each method's performance are explained in **section 5.3**. Finally, the results of the different scenarios are discussed with some suggestions on how the algorithms can meet the positioning requirements in 5G systems and beyond in **section 5.4**.

5.1 Generating 5G NR Uplink Waveform

Generating a 5G NR uplink signal was accomplished by using built-in functions in MATLAB 2021a, which offers the 3GPP-compliant configurations. It has been used the FR2 frequency range, commonly known as mm-waves, with a bandwidth of 100 MHz and a grid size of 66 RBs. The multipath signals were generated copies of the Line of Sight (LOS) Signal with an arbitrary attenuation coefficient and delay. The simulation's system parameters are shown in **Table 5.1**.

Table 5.1: Simulation System Parameters

Frequency Band	FR2 (mm-waves)
BW (MHz)	100
SubCarrier Spacing (kHz)	60
Grid Size (RB)	66
Array Antenna	ULA
Interelement distance (m)	λ/2
Center Frequency (GHz)	28

Noise	AWGN
Channel Impairment	Multipath
# of Paths	{1:7}

As mentioned previously in this section that SRS is the main signal used to test the algorithms during the simulation. The configuration of the SRS signal according to the 3GPP specification [56] is used, as shown in **Table 5.2**. The resource allocation for the SRS signal is shown in **Figure 5.1**.

Table 5.2: SRS Configuration

SRS Symbols	4
Transmission comb size K_{TC}	4
Symbol Start	0
Cyclic Shift	0
Bandwidth configuration C_{SRS}	12
B_{SRS}	0
Period	10
Repeat	1

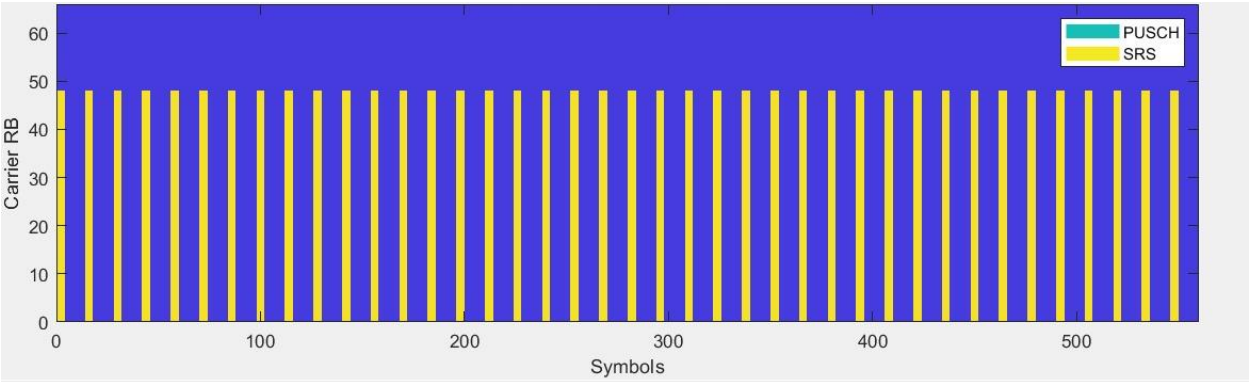

Figure 5.1: Rescource allocation for SRS

5.2 Algorithms Implementaiton

All algorithms are implemented in MATLAB according to the steps of the algorithms provided in **section 4**. Below are some modifications and parameters used to achieve the best possible performance:

- The scanning step in all algorithms that require scanning is set to 0.05.
- The MVDR method was modified using the Moore–Penrose inverse, a generalization of the matrix inverse since MVDR suffers when attempting to compute the inverse of the covariance matrix when it becomes a singular matrix.
- The FFT method was modified by taking the FFT $\mathbf{N}$ times and averaging the spatial spectrum.
- The CASCADE method uses $\pm 10^{o}$ Angle margin.
- CASCADE LOS focuses only on the Line of Sight (LOS) detection.

5.3 Evaluation Metrics

Section four highlighted that most of the algorithms are based on detecting the peaks from the spatial spectrum. Thus, the first section of the simulation evaluates and presents the algorithms' spatial spectrums. All algorithms were evaluated by monitoring their spatial spectrum, which provides sufficient information about the algorithm's accuracy, resolution, and ability to detect Line of Sight (LOS) as well as the multipath signals. The spatial spectrum represents the signals in the spatial domain (i.e., the direction of the signals). The x-axis represents the azimuth angle that we aim to estimate, while the y-axis represents the algorithm's normalized power. Different from other techniques, the ESPRIT method is not based on the spatial spectrum and can resolve angles directly without searching for and identifying peaks. The estimated angles by ESPRIT have been indicated in the same plot at zero dB to incorporate ESPRIT in this comparison.

The resolution is defined as the minimum angle difference between two adjacent angles, while the accuracy is the minimum estimation error in the measurement. The algorithm's performance was assessed with different scenarios of the algorithms' parameters: number of antenna elements, SNR, and snapshots (samples).

The accuracy metric used throughout the simulation was Root Mean Square Error (RMSE) because it utilizes the same units as the quantity displayed on the vertical axis (i.e., a degree in our simulation) [57]. It is also a widely used metric for estimating AoA; for instance, it was used in [51],[26], and [58]. The following formula gives the root mean square error:

$$\boldsymbol{RMSE} = \sqrt{\frac{\sum_{k=1}^{r}\left(\widehat{\boldsymbol{\theta}}_{k} - \boldsymbol{\theta}_{true}\right)^{2}}{\boldsymbol{r}}} \qquad (\mathbf{5.1})$$

Where,

r is the number of trials,

$\widehat{\boldsymbol{\theta}}_{\boldsymbol{k}}$ is the estimated Angle,

$\boldsymbol{\theta}_{\boldsymbol{true}}$ is the actual Angle.

It is worth noting that only LOS was examined for RMSE since that is our primary focus in positioning; nevertheless, there are presently numerous attempts in the research community to use multipath signals for positioning; nonetheless, that is beyond the scope of this thesis. In this study, it was considered that the strongest signal is the line of sight.

A careful study of the necessary number of floating-point operations (FLOPs) is often required when designing efficient and low-complexity algorithms for a variety of signal-processing applications. The complexity of each algorithm in terms of the number of floating points is derived by [34] and, depending on the approach introduced by [59], is shown in **Table 5.3**.

Where,

$\boldsymbol{M}$ is the number of antenna elements,

N is the number of snapshots,

$\boldsymbol{K}$ is the number of the multipath signals,

$\boldsymbol{N_{FFT}}$ is FFT length,

$\boldsymbol{S}$ is the searcing length,

$\boldsymbol{S_{CAS}}$ is the minimized searching length in the CASCADE method.

Assuming $\boldsymbol{M}$ is constant, the most critical variable of the complexity, as shown in **Table 5.3**, is the number of search steps $\boldsymbol{S}$. For example, if we search from -90 to 90 and the searching step is 0.01, this variable will be 18001. Reducing $\boldsymbol{S}$ to $\boldsymbol{S_{CAS}}$ will result a noticibal decreasing in the running time of the algorithm; for that reason, the CASCADE method was proposed.

When it came to the number of snapshots $\mathbf{N}$, the author in [34] considered computing the covariance matrix using **Eq 4.13**, even though the amount of FLOPS is counted, the vectorization method of executing **Eq .4.13** will substantially decrease the time. Also, it can be noticed that the complexity of the modified FFT algorithm increases $\mathbf{N}$ times than the original FFT since we are computing the spatial spectrum $\mathbf{N}$ times.

Table 5.3: Float Operations for AoA algorithms.

BeamForming	$\boldsymbol{M^2(\mathrm{N}+2)+M+4\,KS}$
MVDR	$\boldsymbol{M^2(\mathrm{N}+6)+M+4KS}$
MUSIC	$\boldsymbol{\frac{5}{3}M^3+M^2(\mathrm{N}+1+K+M)+4KS}$
ESPRIT	$\boldsymbol{M^2\left(\mathrm{N}+\frac{6M}{3}+1\right)+K(K+1)}$
FFT	$\boldsymbol{(N_{FFT}\,log(N_{FFT})+4K(N_{FFT}))\ *\mathrm{N}}$
CASCADE	$\boldsymbol{(N_{FFT}\,log(N_{FFT})+4K(N_{FFT}))\ *\mathrm{N}+\frac{5}{3}M^3+M^2(\mathrm{N}+1+K+M)+4KS_{CAS}}$

For practical realization, each algorithm's run time or processing time was used to quantify the algorithm's complexity during the simulation. Because the running time might change slightly according to the running background applications in the computing device, it was proposed to take $\boldsymbol{r}$ trials and average the result for more precise results.

The following formula was used to measure the elapsed time metric:

$$\boldsymbol{ELTM}\ =\frac{\sum_{k=1}^{r}\left(\mathrm{T}_{End}(k)-\mathrm{T}_{Start}(k)\right)}{r} \qquad (5.2)$$

Where,

$\boldsymbol{ELTM}$ is the elapsed time metric in seconds,

T_{End} is the recorded time after executing the last line of the algorithm,

T_{Start} is the recorded time at the beginning of the algorithm, and

$\boldsymbol{r}$ is the number of trials.

5.4 Results

This sub-section concerns the results of the simulation by using the metrics, as illustrated in **section 5.3**. The simulation was divided into three main parts.

The first is comparing the algorithms by their spatial spectrum with different scenarios to check how the spatial spectrum is different from one algorithm to another and how the peaks can be identified from the spectrum. The second is the comparison by the accuracy of detecting and correctly estimating the LOS with inspecting the impact of the number of

antenna elements ($\boldsymbol{M}$), Signal to Noise ratio (**SNR**), and the number of snapshots (**N**). For the third part, the algorithms' complexity in terms of each algorithm's runtime was measured and presented versus the number of antenna elements ($\boldsymbol{M}$), and the number of incoming signals ($\boldsymbol{K}$).

5.4.1 Spatial Spectrum Results

Six scenarios were created to investigate the spatial spectrum are listed in **Table 5.4**. The scenarios have been chosen to cover all the parameters that might affect the performance of the algorithms.

The first scenario explains how to extract information from the spatial spectrum; therefore, the parameters have been set to ensure that all algorithms run smoothly, and the angles are resolved. The number of snapshots (samples) was set to 100, the number of antenna elements was 32, and the SNR was set to 10 dB. The second scenario tests the algorithms' performance when only four snapshots are taken. In the third scenario, the impact of low SNR is investigated. In scenario four, the algorithms are tested with a massive antenna (e.g., 128). Section five indicates how the algorithm can resolve closed signals where the incoming signals test the algorithms with angles of 0^o, and 2^o . In the 6th scenario, the algorithms are tested to see whether they can resolve signals near the spectrum's edge (e.g., 90^o).

As previously stated in the thesis, each algorithm's mathematical model is different, leading to diverse behavior and performance versus those parameters. For instance, MVDR relies on the inverse of the covariance matrix ($\boldsymbol{R_{XX}}$) as stated in **Eq. 4.13**; however, if $\boldsymbol{R_{XX}}$ Becomes singular (mainly because of the correlation between the incoming signals), the matrix has no inverse, leading to error in the Estimation.

Table 5.4: Spatial Spectrum Scenarios

	Scenario 1	**Scenario 2**	**Scenario 3**	**Scenario 4**	**Scenario 5**	**Scenario 6**
Number of signals $\boldsymbol{K}$	2	2	2	2	2	2
Number of Snapshots **N**	100	4**	100	100	100	100
Number of antenna elements $\boldsymbol{M}$	32	32	32	128	32	32
Signal-to-Noise ration SNR [dB]	10	10	-15	10	10	10
Azimuth angle **θ** [Degree]	{**0***,60}	{**0**,60}	{**0**,60}	{**0**,60}	{**0**,2}	{**88,70**}
FFT Size	512	512	512	512	512	512

**The underlined-bold angle represents the line of sight.*

***Scenario 2 assumes the two signals arrive at the same time.*

5.4.1.1 Spatial Spectrum Scenario 1: Describing the Spatial Spectrum (SS)

The first scenario depicts the spatial spectrum of all algorithms in a moderate environment with a large number of snapshots and 32 antenna elements, ensuring that all algorithms run smoothly, and angles can be resolved. In this scenario, we are looking to identify the two signals, the line of sight (LOS) at 0^o and another multipath signal assumed to impinge at an angle of 60^o. **Figure 5.2** depicts the spatial spectrum of all algorithms. It can be seen that all algorithms succeeded to detect the two paths, where the first peak corresponds to the LOS at 0^o and the reflected path is at 60^o. However, this judgment is governed by whether we know the number of incoming signals or not. This is mostly due to the fact that certain algorithms include more than two considerable peaks, such as the BF and FFT techniques. The signal detection methodology depends on the strength of the incoming signals, as mentioned at the beginning of the section. That is, the highest level corresponds to LOS. Other methods for channel estimation and time delay estimation utilizing SRS signals for the purpose of detecting multipath signals are not addressed in this research. In **Figure 5.2**, the BF and FFT Spatial Spectrum contain additional (yet smaller) peaks than other estimation techniques, which increases the uncertainty in angle measurement, particularly if the number of incoming signals is unknown. As predicted, MVDR coped with the BF problem by imposing constraints on other directions, as stated in **section 4.2.2**.

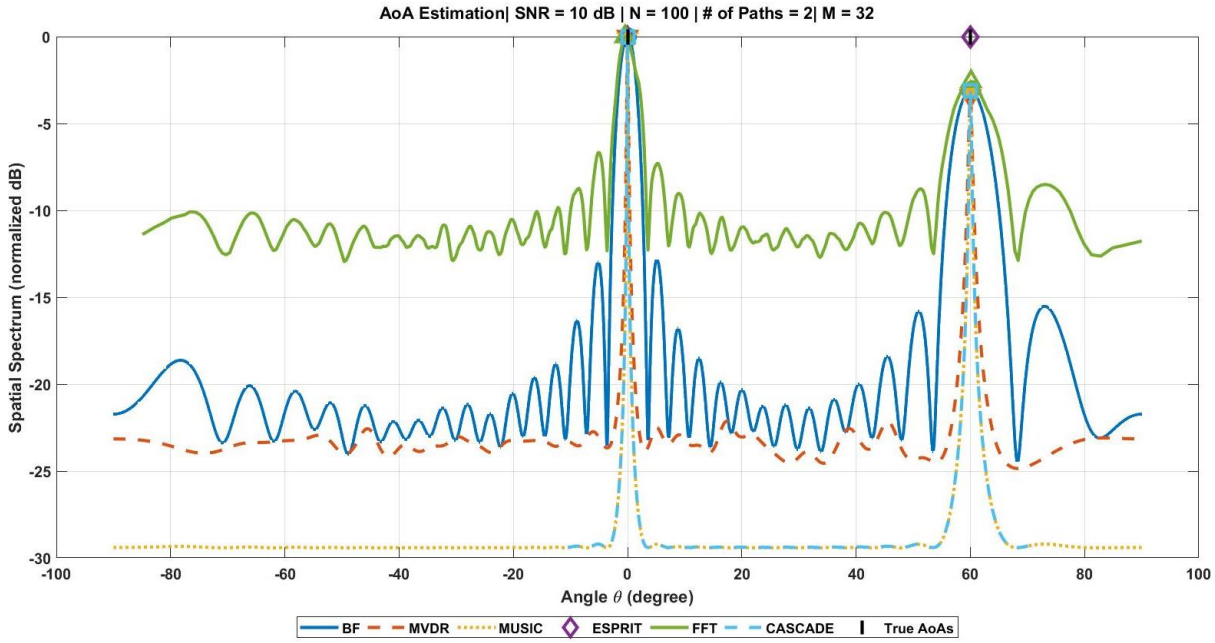

Figure 5.2: Spatial Spectrum Scenario 1 (Describing the Spatial Spectrum). SNR=10 dB, N=100,M=32, FFT size=512,K=2, True angles={0,60}.

The MUSIC algorithm has a clear and smooth spatial spectrum with only two peaks, as it is well-known as a super-resolution algorithm. The proposed CASCADE algorithm minimizes the searching region and produces an almost identical spectrum to that of MUSIC. The highest $\boldsymbol{K}$ peaks have been marked with markers since we had previous information about the number of signals throughout the simulation.

5.4.1.2 Spatial Spectrum Scenario 2: Impact of the number of snapshots (N)

This scenario concerns the impact of the number of snapshots on the spatial spectrum. Generally, more snapshots mean more accurate covariance matrix estimation, leading to better accuracy and resolution. Except for $\mathbf{N}$, which was adjusted to four, the parameters from the first Scenario were maintained as in **Table 5.4**. The delay of the reflected signal was also assumed to be zero. The purpose of this is to guarantee that both signals are within the first four samples; otherwise, the simulation would only include zeros for the

second signal. **Figure 5.3** shows how the performance deteriorated with only four samples (**N** = 4). This deterioration is because all the algorithms use a covariance matrix as an early step in the algorithm for the estimation, except the FFT algorithm, which can be improved by increasing the array elements. It is worth mentioning, the spatial spectrum of the FFT method also degrades when the number of snapshots is decreased because it was utilized a modified FFT algorithm that takes **N** snapshots and determines the spatial spectrum for each snapshot before averaging them.

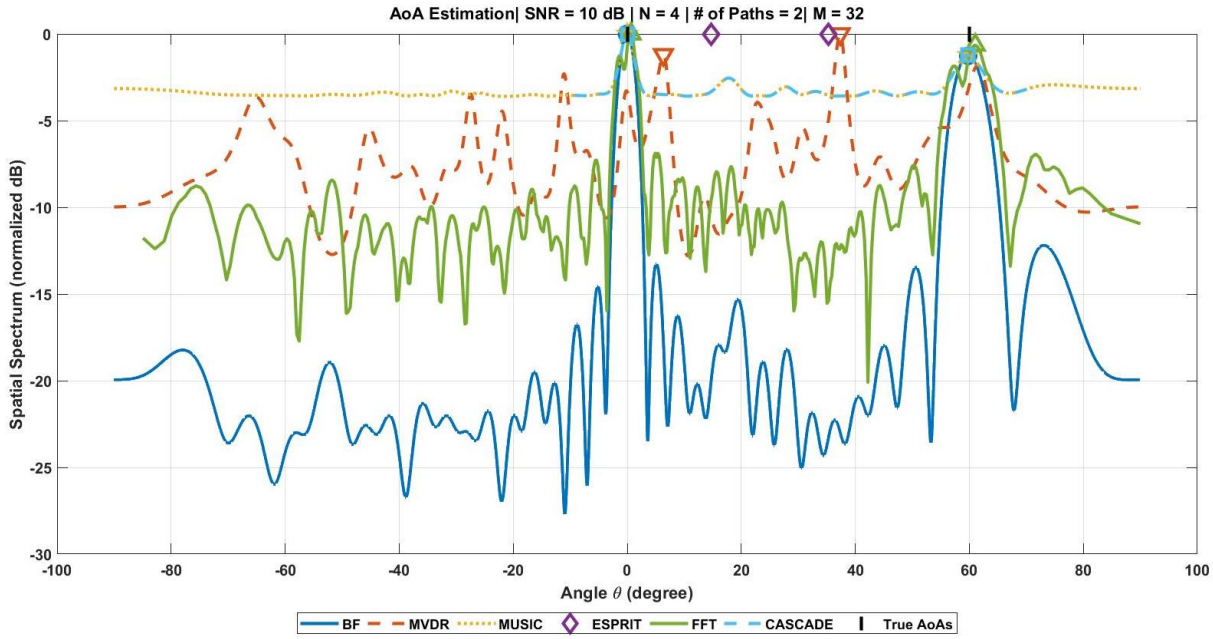

Figure 5.3: Spatial Spectrum Scenario 2 (Effect of Snapshots on Spatial Spectrum). SNR=10 dB, N=4,M=32, FFT size=512,K=2, True angles={0,60}.

5.4.1.3 Spatial Spectrum Scenario 3: Impact of the SNR

In this scenario, a low signal-to-noise ratio (SNR) was assumed in order to investigate the impact of SNR. SNR was set to -15 dB using the same settings as the prior two scenarios. The results of this scenario are shown in **Figure 5.4**.

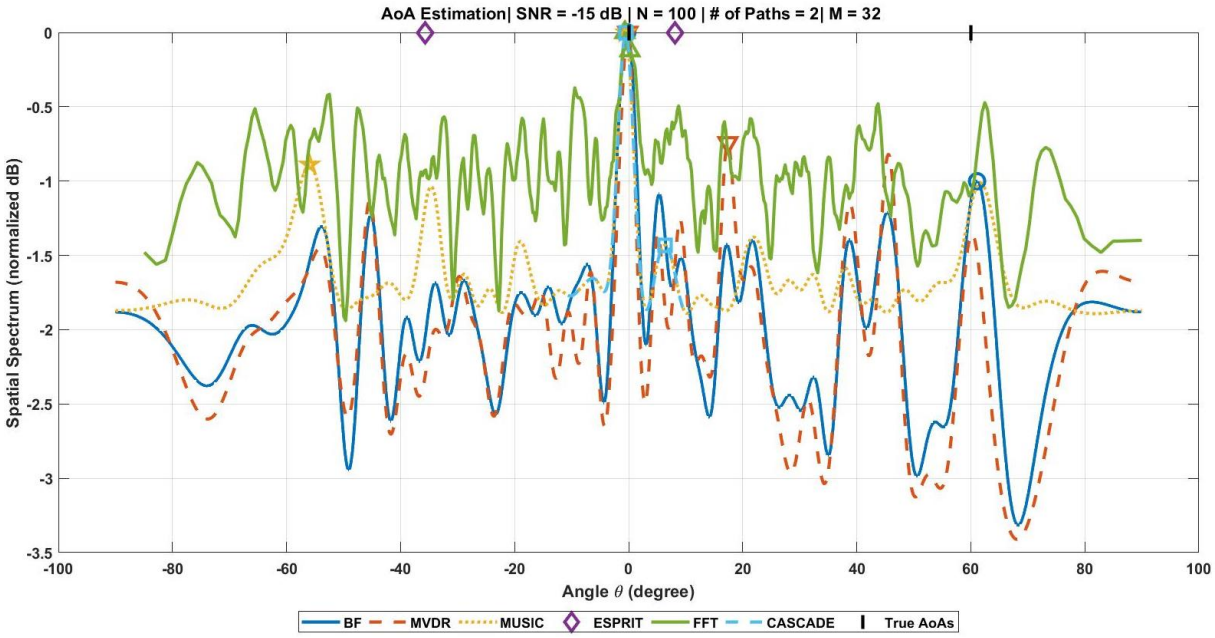

Figure 5.4: Spatial Spectrum Scenario3 (Effect of SNR on Spatial Spectrum). SNR=-15 dB, N=100,M=32,FFT size=512,K=2, True angle={0,60}.

The figure shows that when the SNR dropped to -15 dB, which is considered low SNR, all techniques performed poorly; nevertheless, the Angle of the LOS signal could still be resolved. This degradation in the spatial spectrum is primarily due to a deterioration in the covariance matrix, which increases the level of side loops, resulting in a reduction in BF and MVDR performance. For the FFT, as the input signal becomes distorted with a high noise level, the side loops become increasingly noticeable. This degree of SNR altered the spatial spectrum even for the superresolution techniques (i.e., MUSIC, ESPRIT, and CASCADE). The spatial spectrum for MUSIC and CASCADE now contains numerous peaks as a result of this environment. This deterioration in the spatial spectrum came from the assumptions made when we mathematically derived the subspaces that the smallest eigenvalues corresponding to the noise are no longer valid since the noise power has been increased (i.e., low SNR). This leads to errors in the estimation of the signal and noise subspaces, which reduces the performance of MUSIC, CASCADE, and ESPRIT. Additional studies of SNR's impact on LOS are provided later in light of the RMSE metric in **section 5.4.2**.

5.4.1.4 Spatial Spectrum Scenario 4: Impact of the number of array elements (M)

The mmWaves are the new range of frequencies standardized in 5G systems, which opened the way for using more antenna elements to mitigate the propagation loss and increase the directivity of the beam. After Massive MIMO, a new portion of the frequencies in the Terahertz range is being investigated as one of the expected enabling technologies in 6G and beyond. This increase in antenna elements will play a significant role in the Angle of Arrival estimation problem. Generally, the more antenna elements, the better accuracy, but this improvement is not free and perfect in all aspects. The complexity of the algorithm described by the processing time will be increased dramatically for most traditional algorithms, as explained in **Table 5.3**. In this scenario, 128 array elements were employed, the algorithms' responses are presented in **Figure 5.5**. The spatial spectrum in the Figure shows that as $\boldsymbol{M}$ increased, the beams became narrower for all methods. Side loops are almost eliminated in MVDR, MUSIC, and the proposed CASCADE method. Nonetheless, the additional loops are still present in the spatial spectrum with a small beamwidth in FFT and BF methods.

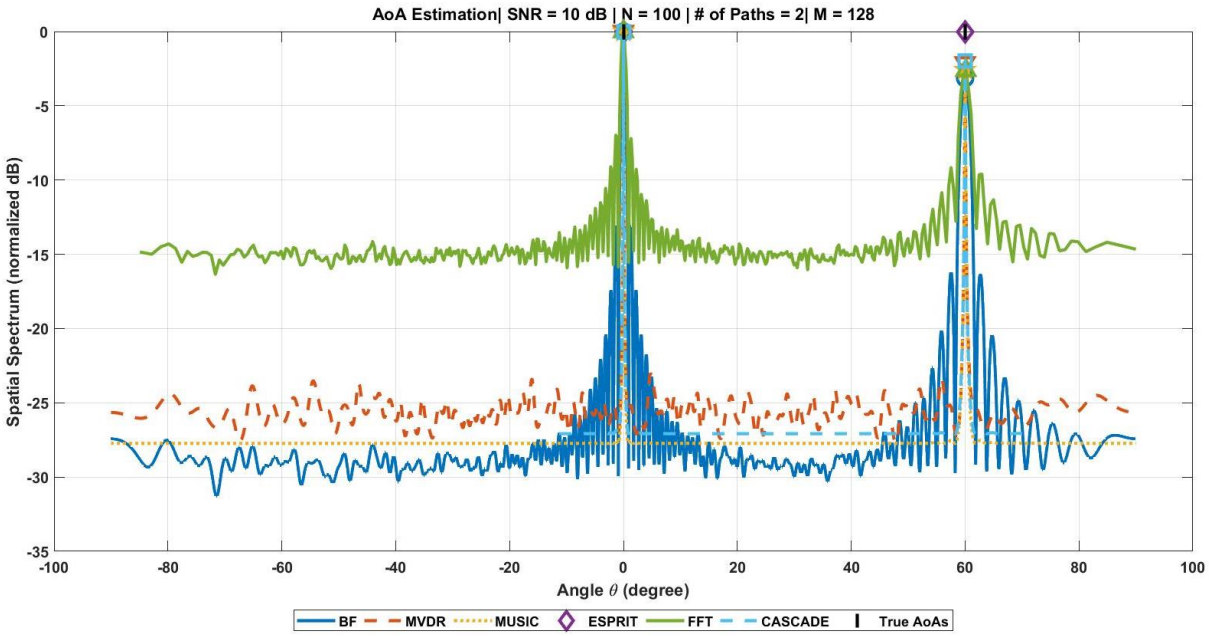

Figure 5.5: Spatial Spectrum Scenario 4 (Impact of M on Spatial Spectrum). SNR=10 dB, N=100,M=128, FFT size=512,K=2 True angles={0,60}.

5.4.1.5 Spatial Spectrum Scenario 5: Resolution

This Scenario tests the resolution of the algorithm by receiving two spatially closed incoming signals at 0^o, and 2^o For the Line of Sight, and the reflected signal, respectively, with a high value of SNR and 32 array elements. **Figure 5.6** shows the result of this scenario. From the result, the MUSIC algorithm, ESPRIT, and the proposed CASCADE method correctly measured the three closed signals' angles.

BF and FFT algorithms failed in this test due to their wide beamwidth, which results in poor resolution. MVDR succeeded in estimating the signal correctly but with low accuracy for the second signal. From the preceding scenarios, it can be inferred that increasing the number of snapshots or/and the number of array elements can enhance the resolution of the algorithms.

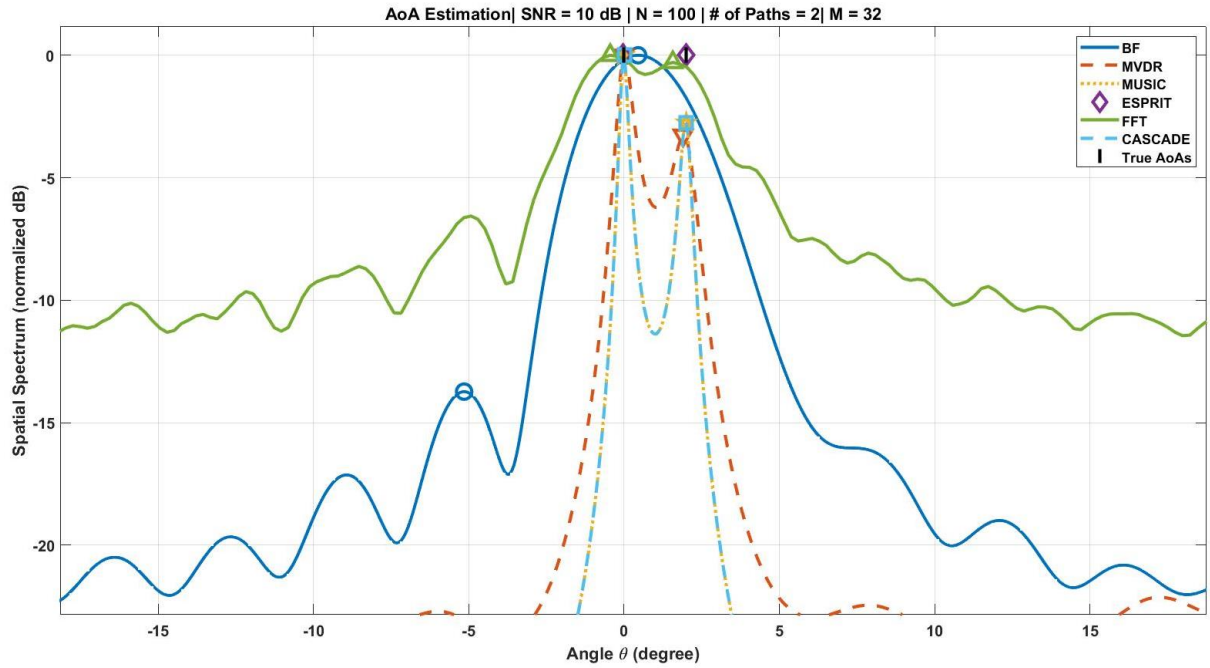

Figure 5.6: Spatial Spectrum Scenario5 (Resolution of the Spatial Spectrum). SNR=10 dB, N=100,M=64,FFT size=512,K=2 True angles= {0,2}.

5.4.1.6 Spatial Spectrum Scenario 6: Closing to the edge of the spectrum

This scenario investigates the performance of the algorithms when the signals arrive at angles close to the spectrum's edge. The spectrum range for uniform linear array (ULA) is from -90^o to 90^o. The algorithms might incorrectly estimate AoA when the signals arrive at an angle close to the limit of that range. To this end, this scenario aims to examine how algorithms behave when the impinging signals are close to that limit (e.g., 88^o).

Two incoming signals with an angle of 88 and 70 were considered in this scenario, SNR was set to 10, 32 array antenna elements were used, and 100 snapshots were taken. The results of this scenario are shown in **Figure 5.7**.

The simulation results show that ambiguity is raised when the AoA is close to the spectrum's edge. BF and FFT have, as usual, many peaks, and the spectrum is symmetric. BF failed to detect the second signal correctly. The spatial spectrum for each of MUSIC, MVDR, and FFT is unclear as it is symmetric, raising the ambiguity. The CASCADE has the best spectrum among all the methods as it removes that symmetry when it minimizes the scanning region. Even though all algorithms detect the LOS, there is still a high chance of increasing the error if the condition changes (e.g., low SNR).

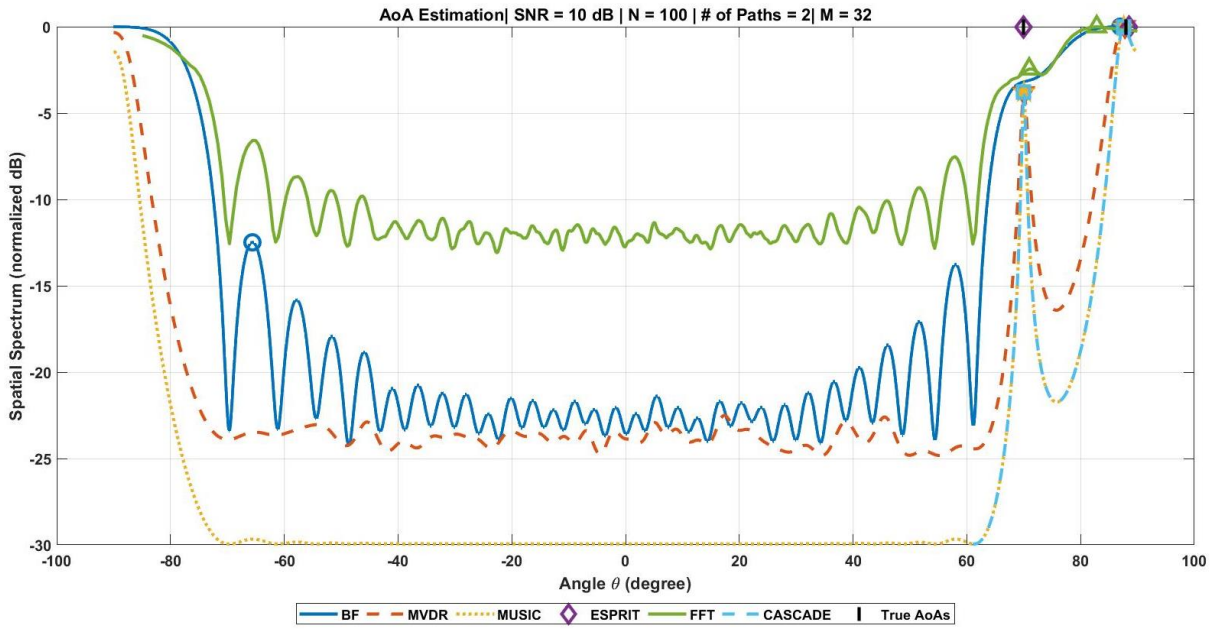

Figure 5.7: Spatial Spectrum Scenario 6 (Closing to the edge). SNR=10 dB, N=100,M=32,FFT size=512,K=2, True angles={88,70}.

5.4.2 Root Mean Square Error (RMSE)

The spatial spectrum in the previous sub-section can describe the resolution and accuracy in different conditions; nonetheless, that degree of accuracy from the spatial spectrum is not enough to pick one algorithm among the others to assign it as the best one for particular use cases. RMSE metric, as given in **Eq. 5.1**, can be used to track the accuracy against those parameters described in the previous section for r trials. Hence RMSE was used in this second part of the simulation to inspect the algorithm's performance against the main parameters affecting estimation accuracy, such as SNR.

The main focus in this sub-section is the LOS; therefore, RMSE was calculated for only the LOS. RMSE measurements have been divided into three Scenarios as following:

1. RMSE-SNR with four different values of antenna elements M
2. RMSE-SNR with four different values of N.
3. RMSE-Number of incoming signals K.

Table 5.5 shows the simulation parameters for the three scenarios mentioned above.

Table 5.5: RMSE Scenarios

Parameter	Scenario 1	Scenario 2	Scenario 3
Number of signals K	fixed = 2	fixed = 2	1:2:9
Number of Snapshots N	fixed = 100	{1,10,100,1000}	fixed = 100
Number of antenna elements M	{8,16,32,64}	32	fixed= 32
Signal-to-Noise ration SNR [dB]	-20:4:20	-20:4:20	fixed = 10
Azimuth angle θ [Degree]	{60,70}	{60,70}	{-70, -60, -50, -40, -30}
FFT Size	fixed = 1024	fixed = 1024	fixed = 1024
Number of Trials	fixed = 60	fixed = 60	fixed = 60

5.4.2.1 RMSE Scenario 1: Impact of the number of array elements M and SNR

This Scenario explores how the algorithms behave the increase in the number of array elements in 5G systems and beyond in terms of accuracy. More growth in using antenna elements, especially in the mm-Waves range, is expected to be available in 5G and beyond to mitigate the propagation loss by increasing the directivity of the antennas. To monitor the impact of noise on estimate accuracy, the RMSE was computed for each value of M in a range of SNR. In general, the more antenna elements there are, the better the estimation accuracy. However, as shown later in **section 5.4.2.1**, these enhancements improve accuracy at the expense of complexity, which implies that increasing the number of array components substantially increases the complexity of most algorithms.

In this simulation, two signals, a line of sight and a reflected signal, were generated and processed as the algorithms' input, implying that the signals are correlated to make the simulation more realistic. The signal-to-noise ratio was adjusted to be between -20 and 20 dB, and the number of snapshots was set at 100. FFT has a length of 1024, and the simulation is repeated four times with various values of M and 60 trials at each value of SNR. **Table 5.5** lists all of the parameters for this simulation.

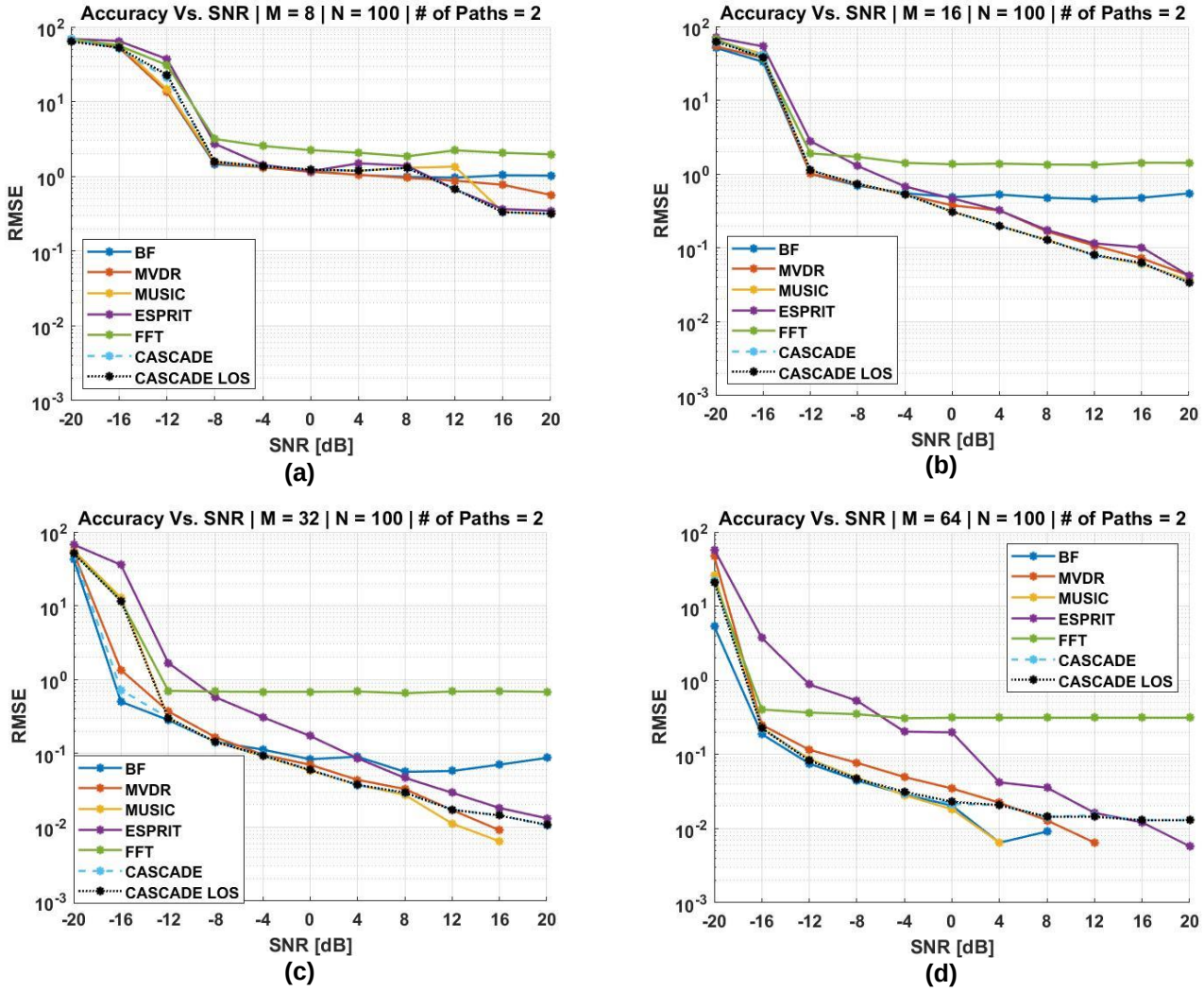

Figure 5.8: Accuracy Vs. SNR with different values of M, N=100,M={8,16,32,64},FFT size=1024,K=2, True angles = $\{60^o, 70^o\}$.

Figure 5.8 shows the algorithms' accuracy vs. SNR for a different number of array elements (M). In **Figure 5.8 (a),** 8 elements are used; The figure shows that below -8 dB SNR, BF, and MVDR surpass the other methods marginally or have the same accuracy.

However, when the SNR rises, MUSIC, ESPRIT, and CASCADE are as accurate as BF and MVDR. MUSIC, and CASCADE outperform BF and MVDR and have the same accuracy as ESPRIT when the SNR is above 12 dB. When SNR rises, FFT improves somewhat. In **Figure 5.8 (b),** 16 antenna elements were used, and all other parameters were kept unchanged. It can be noticed that when $\boldsymbol{M}$ changed from 8 to 16, all algorithms performed better. BF, MVDR, MUSIC, and CASCADE are very close to be identical at below -4 dB SNR. However, when SNR is higher than -4 dB, MUSIC and CASCADE noticeably surpass BF and FFT and slightly outperform MVDR and ESPRIT. Again, by keeping increasing the number of antenna elements, all algorithms' estimation accuracy improves. CASCADE LOS is the same as CASCADE but focusing on estimating the LOS. It can be noticed from the figures that MUSIC, CASCADE, and CASCADE LOS have identical accuracy.

The FFT technique offers modest accuracy; nevertheless, this Degree of accuracy improves when using more antennas, like in ultra-massive MIMO (e.g., 256, 512, 1024). Furthermore, the Figure shows that FFT is not as influenced by SNR as the others; nevertheless, its accuracy varies directly with the number of antenna elements. This feature gives motivation to further refining this technique to enhance its accuracy, particularly by giving a large array antenna that can be used for enhanced AoA measurements.

5.4.2.2 RMSE Scenario 2: Impact of the Snapshots ($\mathbf{N}$) and SNR

This Scenario focuses on how the number of snapshots affects the algorithm's performance. The simulation settings were configured as indicated in **Table 5.5.**

Figure 5.9 illustrates how the number of samples affects the accuracy of algorithms with various $\mathbf{N}$ **,** and using an SNR range of -20 dB to 20 dB.

Figure 5.9(a) depicts the accuracy when just a single sample is taken into consideration. According to the result, it can be seen that MVDR has the lowest accuracy among all the algorithms. The accuracy against SNR is shown in **(b)**, **(c)**, and **(d)** for 10,100 and 1000 samples, respectively. The RMSE-SNR results improve intuitively as $\mathbf{N}$ increases due to improved construction of the covariance matrix since we are using an estimated one. It is worth noting that the FFT technique is based on just collecting one sample. However, it was modified in this simulation to take $\mathbf{N}$ snapshots and then take the average of the spatial spectrum before locating the peaks.

As a result, it can be shown that as $\mathbf{N}$ increases, these techniques improve. The findings also show that, at low SNR, the BF technique performs slightly better than the CASCADE method, while at high SNR, the CASCADE method surpasses the BF. ESPRIT has poor performance with just a few snapshots, particularly at low SNR, making it a bad option for applications requiring only a few samples. Finally, the MUSIC algorithm is almost identical to the CASCADE method.

From the results of this section and the previous section, it can be noticed the following:

- BF marginally performs better than the other in very low SNR (<-8 dB).
- MUSIC, CASCADE, and CASCADE LOS have almost identical accuracy.
- MVDR is the most affected algorithm when taking few samples.
- BF and FFT can be improved considerably by increasing the number of antenna elements because when 32 antenna elements were used and 1000 samples in **Figure 5.9 (d),** the BF didn't reach that accuracy level when used 64 antenna elements and 100 samples in **Figure 5.8 (d).** This means the most significant parameter for BF and FFT is the number of antenna elements.

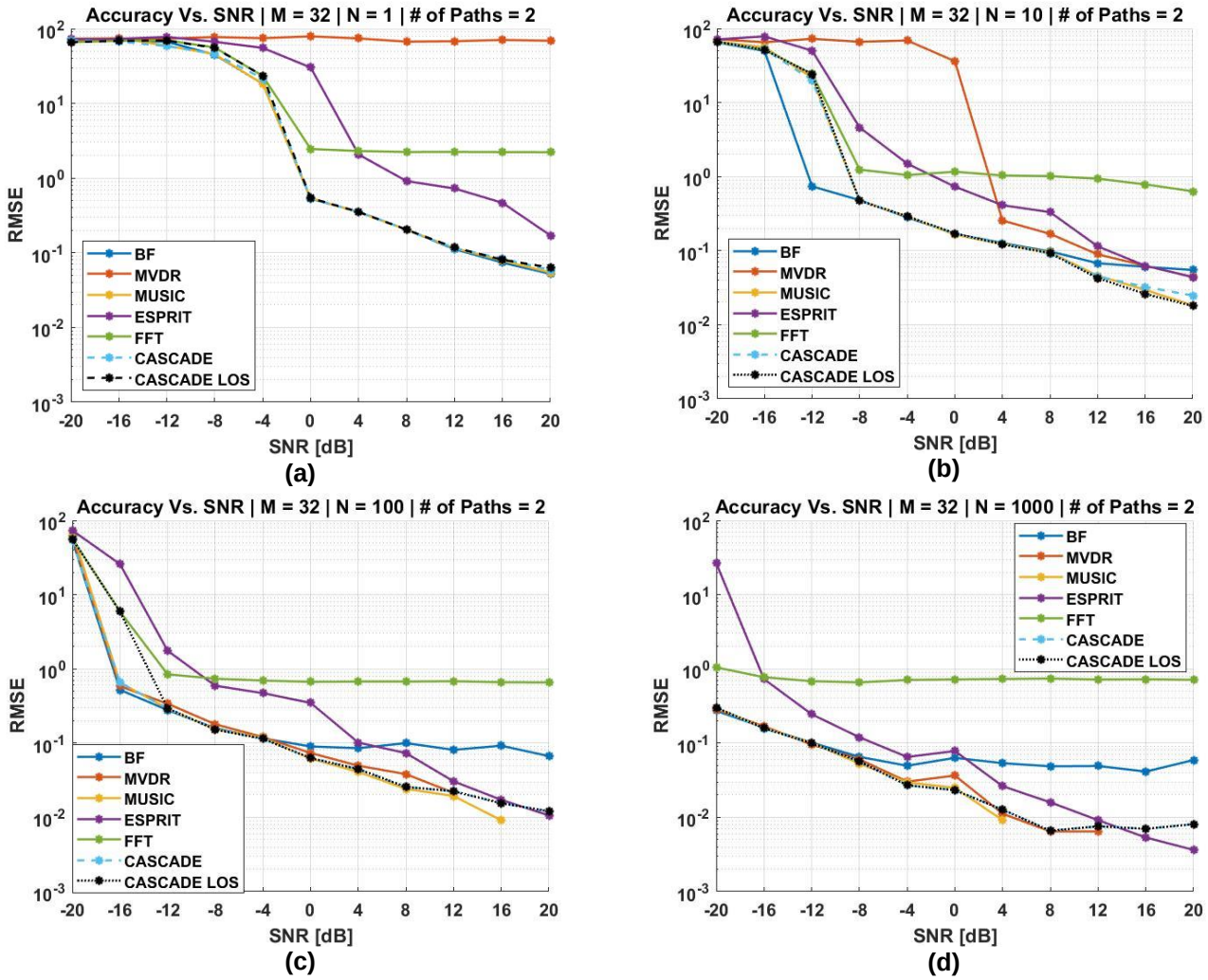

Figure 5.9: Accuracy Vs. SNR with different values of N, M = 32, N={1,10,100,1000},FFT size=1024,K=2, True angles = {$60^o, 70^o$}.

5.4.2.3 RMSE Scenario 3: Impact of the correlated sources (K)

This Scenario examines the impact of the number of sources (incoming signals) on algorithms' performance. The RMSE was computed by increasing the number of multipath signals. The simulation settings for this scenario are indicated in **Table 5.5.**

As demonstrated previously in section four, the super-resolution and MVDR algorithms suffer immensely from signal correlation. In MVDR, the covariance matrix becomes singular, leading to an error when computing the inverse of the matrix and an error in the Estimation. MUSIC algorithm and ESPRIT relays on eigenvalue decomposition (EVD). EVD assumes that the covariance matrix is a full rank matrix; however, the covariance matrix will become rank deficient with the presence of the correlated signals. This will lead to an error in the estimation and identifying the peaks. As multipath signals, all tested signals were correlated throughout the simulation (copies of the LOS).

The RMSE results against the number of sources $\boldsymbol{K}$ are depicted in **Figure 5.10**.

The results of this simulation show that the more correlated the sources, the lower the estimate accuracy. ESPRIT performs the poorest in this test, which is due to two reasons. First, it is similar to MUSIC in that it depends on the covariance matrix, but the matrix is no longer a full-rank matrix, and second, it is based on the signal subspace rather than the noise subspace, as is the case with the MUSIC method. That is, more correlated signals increase the error in estimating the signal subspace, resulting in a huge error in estimation. The accuracy of MUSIC and CASCADE degraded severely when the number of sources became 5. FFT has a unique feature in that its accuracy is not affected by the

number of correlated signals, which implies that a few snapshots and a large number of antenna elements may give a considerable performance for many applications. The CASCADE LOS performed the best among all other algorithms which can rely on for practical applications based on LOS detection. Furthermore, the CASCADE LOS algorithm can be modified to estimate not only LOS but rather $\boldsymbol{K}$ multipath signals by segmenting the MUSIC search for each kth peak from FFT spatial algorithm. The result will be a time-efficient and robust algorithm against the correlated multipath signals.

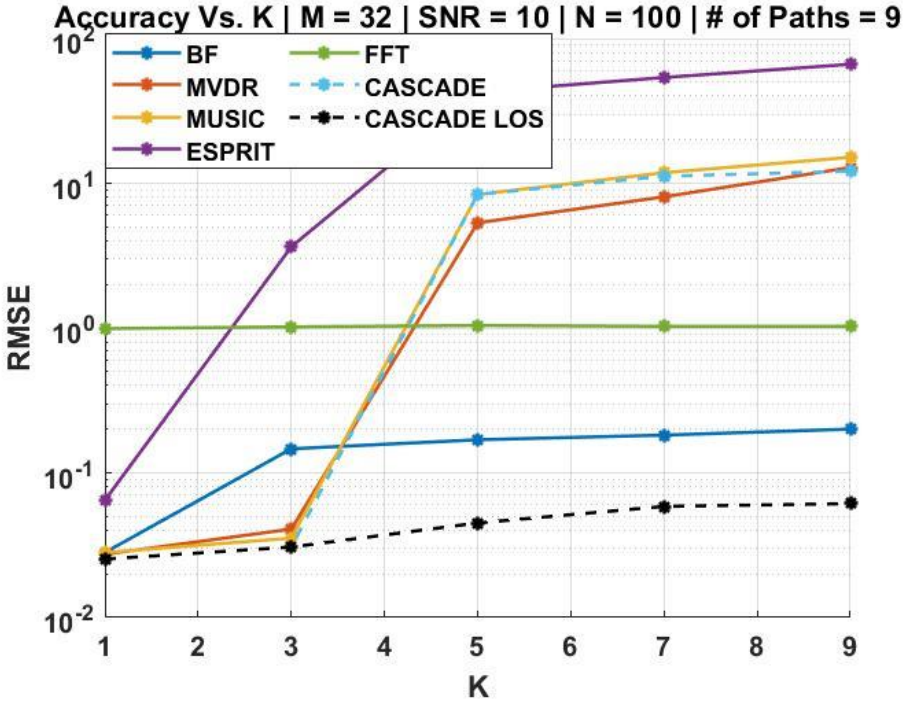

Figure 5.10: Effect of the number of sources on the accuracy.

Finally, the correlated signal is a major problem that should be considered when designing new algorithms for AoA estimation or pre-processing the signal before the algorithm. For example, MUSIC with Spatial Smoothing technique [51] to reduce the effect of correlation.

5.4.3 Elapsed Time Metric (ELTM)

This Scenario compares the complexity of the algorithms in terms of the Runtime for each algorithm. To this end, an ELTM (Elapsed Time Metric) was developed to estimate the run time provided in **Eq.5.2**. This simulation was performed under the specifications of the computing device shown in **Table 5.6.**

Giving the specifications as in **Table 5.6** is essential for measuring time since it cannot be assured that the results will precisely match the practical results. This is due to the fact that the computing hardware will be different, and the algorithm will not be implemented realistically using MATLAB but rather in a fast-programming language (e.g., C).

Table 5.6: Computing Device Specifications

Processor	RAM	Hard Drive	Software
Intel(R) Core(TM) i7-8550U CPU @ 1.80GHz 1.99 GHz	16.0 GB	SSD	MATLAB 2021

The ELTM measurements are divided into three Scenarios as follows:

1. ELTM versus $\boldsymbol{M}$.
2. ELTM versus $\boldsymbol{K}$.

Table 5.7: ELTM Scenarios

Parameter	Scenario 1	Scenario 2
Number of signals $\boldsymbol{K}$	fixed = 2	1:3:15
Number of Snapshots N	fixed = 100	fixed = 100
Number of antenna elements $\boldsymbol{M}$	{8,16,32,64, 128,256}	fixed = 64
Signal-to-Noise ration SNR [dB]	fixed = 0	fixed = 0
Azimuth angle θ [Degree]	{60,70}	{-70, -60, -50, -40, -30,-20, -10 ,0 ,10 20 ,30, 40 ,50}
FFT Size	fixed = 1024	fixed = 1024
Number of Trials	fixed = 60	fixed = 60

5.4.3.1 ELTM Scenario 1: Effect of the number of array elements ($\boldsymbol{M}$)

As demonstrated in **Table 5.3**, the number of array elements is the most critical parameter in the complexity since it increases the number of floating operations in the algorithms. The first Scenario for determining ELTM is to vary the number of array elements $\boldsymbol{M}$ and then compute ELTM for each $\boldsymbol{M}$. **Figure 5.11** illustrates how the running time increases as the number of antenna elements increases.

Except for the FFT technique, all of the methods' elapsed times increase when $\boldsymbol{M}$ is increased. FFT's complexity does not vary as $\boldsymbol{M}$ increases; as a result, as previously stated, this technique may offer significant accuracy in ultra massive antenna systems while having a very low complexity compared to other methods, which can meet a wide range of use cases.

It is worth mentioning that the complexity of CASCADE and CASCADE LOS methods can be further reduced by narrowing the scanning in the MUSIC algorithm by reducing the margin $\boldsymbol{\vartheta}$ in **Eq.4.57**. It was set throughout the simulation as $\pm\, 10^{o}$; however, this is not necessary to be 10. It can be reduced when using large array antennas, and the SNR is high. The justification for setting that margin to ten is to avoid having FFT error near to tens of degrees, which is not the case when utilizing a large array antenna (e.g., 64). Moreover, the FFT algorithm is the first stage of the algorithm, and the consumed time by this stage can be more reduced if we take an average of only ten snapshots instead of 100. Hence, the parameters that govern the CASCADE method need to be selected carefully to ensure the best accuracy in less time.

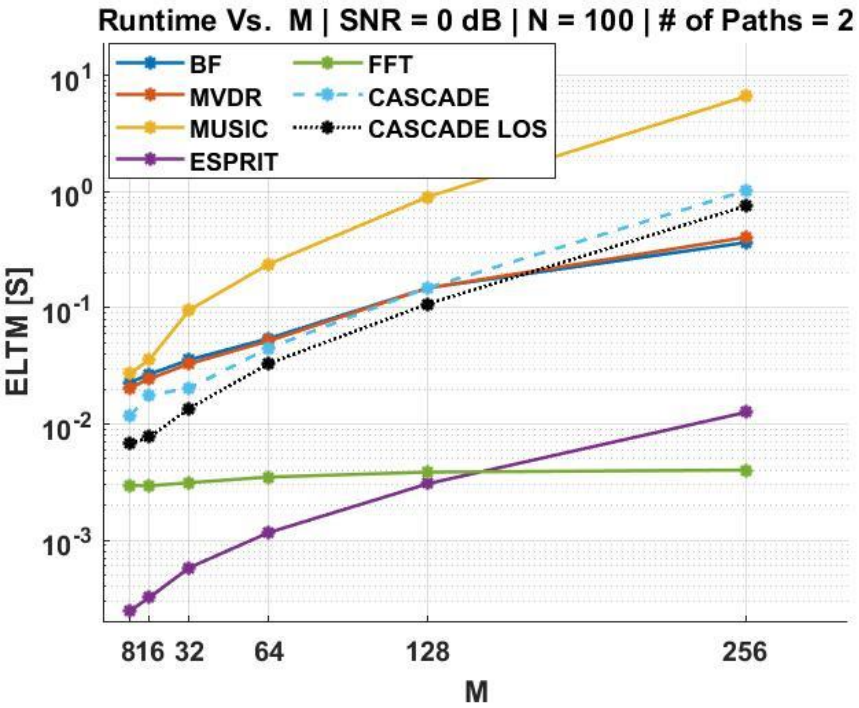

Figure 5.11: Effect of the number of array elements on the complexity.

5.4.3.2 ELTM Scenario 2: Effect of the number of Sources (K)

Finally, this last simulation concerns the effect of the number of multipath signals on the complexity of the algorithms. The simulation parameters are given in **Table 5.7.**

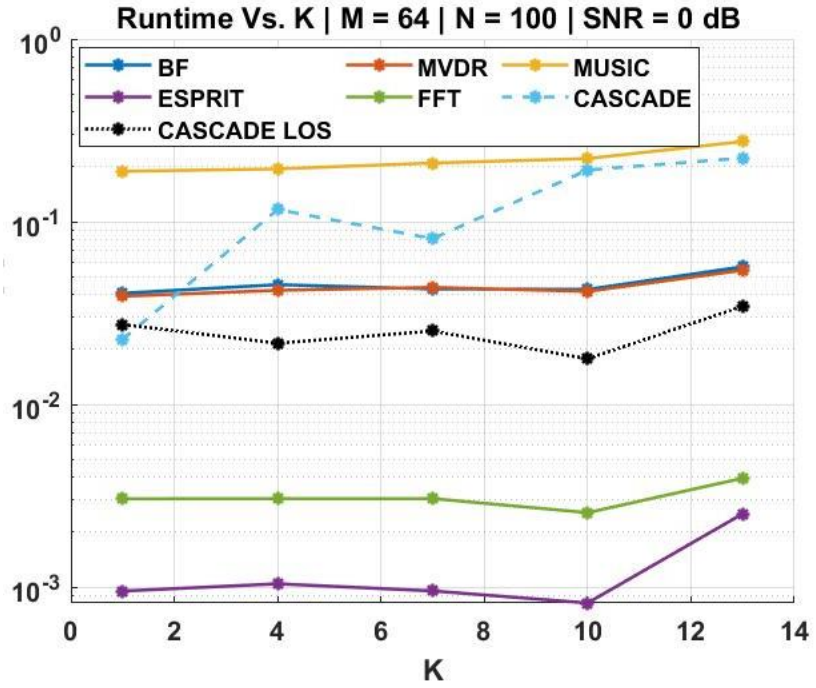

Figure 5.12: Effect of the number of sources on the complexity.

The running time increases as the number of sources increases, as shown in **Figure 5.12**. In this scenario, the CASCADE algorithm is the most impacted one. This is because when there are many signals, it implies there are more picks, which leads to an increase in the scanning area of CASCADE's second stage. As a result, the degree of complexity rises. This increase in the number of signals affects the other algorithms as well; nevertheless, the running time has increased by less than 10%. CASCADE LOS addressed the

CASCADE issue by focusing on just one peak from the FFT spatial spectrum; as a result, there is no substantial rise in ELTM against the number of multipath signals.

5.5 Discussion

Before ending this section, it is crucial to estimate how those measurements of Angle of Arrival meet the requirement of use cases indicated in **section 2.6.**

Assuming that AoA measurement is used for a joint localization algorithm, another positioning measurement technique is employed to measure the distance from the UE to the base station.

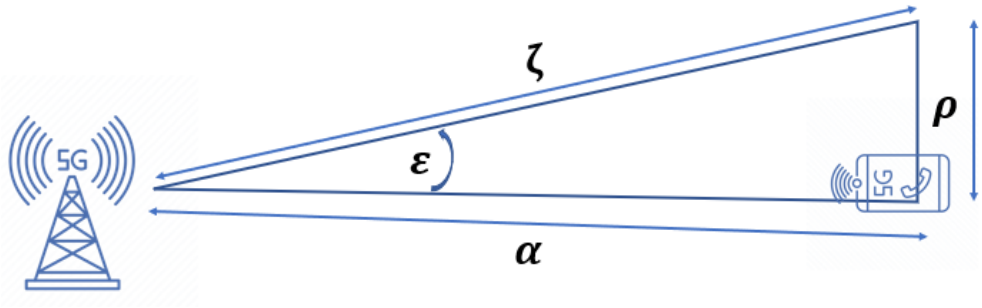

Figure 5.13: Horizontal distance error due to AoA estimation error.

Figure 5.13 shows how the error in AoA denoted by $\boldsymbol{\varepsilon}$ produces an error in the positioning. It is crucial to note that the estimated AoAs throughout this section only provides 1D positioning (i.e., Azimuth angle). In **Figure 5.13,** It is assumed that the range from the base station to the UE is given. Now the approach became 2D positioning, azimuth angle, and distance. $\boldsymbol{\alpha}$ in the figure represents the range from the base station to the UE (known) in m. $\boldsymbol{\zeta}$ is the range from the base station to the point produced due to the error in estimating the angle ($\boldsymbol{\varepsilon}$).

By using the trigonometric equations:

$$\boldsymbol{\rho = \alpha * tan(\varepsilon) * 100} \quad (\mathbf{5.1})$$

$$\boldsymbol{\varepsilon = \theta_{true} - \hat{\theta}} \quad (\mathbf{5.2})$$

Where,

$\boldsymbol{\theta_{true}}$ is the actual AoA,

$\boldsymbol{\hat{\theta}}$ is the estimated AoA,

$\boldsymbol{\varepsilon}$ is the error in the estimation of AoA in (degree), and

$\boldsymbol{\rho}$ is the horizontal error distance (cm).

If $\boldsymbol{\varepsilon}$ is equal to 1^o And the range $\boldsymbol{\alpha}$ is 60 m, the error in horizontal distance $\boldsymbol{\rho}$ is 1.047 m, and when the range $\boldsymbol{\alpha}$ increases, this error will be increased as well.

Figure 5.14 shows how the distance from the base station and the error in AoA lead to increasing the horizontal distance error, leading to an error in the positioning.

Even though this approach can give enough imagination on how the error in AoA estimation impacts the total positioning accuracy in the positioning algorithm, this approach is simple and does not precisely indicate the exact position error corresponding to an error in estimation AoA for two reasons. First, we are estimating only the Azimuth angle, which is not the case practically where the elevation angle needs to be estimated, which means that elevation angle estimation will add an error. Second, we are assuming here a joint localization that requires an accurate estimation of the distance from the base

station to the UE, which might include errors as well. Thus, it is an approximated approach to give an intuition of the maximum allowed error in AoA estimation.

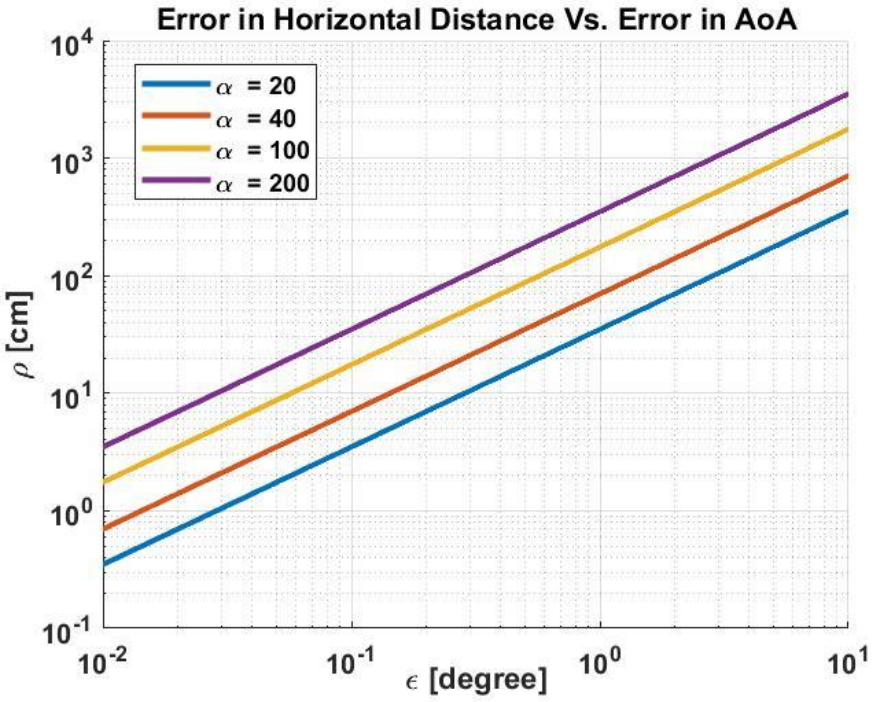

Figure 5.14: Horizontal Distance Error due to AoA error.

The figure above gives an indication that AoA estimation can assist positively in positioning. For example, according to our approach, without including any other errors in estimating the range and without including elevation angle, a 0.1-degree error in estimating AoA will cause only a 3.5 cm horizontal distance error when the distance is 20 m. This level of accuracy can be seen from the AoA estimation results, as shown in the previous sub-sections. For example, when the number of array elements is 64, and the number of the snapshot is 100, this level of accuracy can be obtained when SNR is above -12 dB (excluding the impact of the correlated signals).

As mentioned earlier in **section 2.6**, the requirements in positioning are not only the degree of accuracy. Nevertheless, the required time or latency to localize the UE is of great importance. For instance, **section 2.6** showed the required time ranges from the 30s to 10 ms of most of the use cases.

The AoA estimation might be part of positioning algorithms, for example, a joint localization algorithm or a triangulation algorithm. Therefore, It is essential to measure AoA as little time as possible to ensure that the whole positioning algorithm meets the requirement of the use cases. For example, in the case of using 32 antenna elements $\boldsymbol{M}$, and by taking 100 snapshots, CASCADE LOS resolved AoA in 13 ms. At the same time, the RMSE is less than 0.1^o when SNR is higher than -4 dB, however, MUSIC needed 95 ms to estimate AoA at that degree of accuracy. MVDR and BF required more than 33 ms to find that AoA. ESPRIT is a high-speed algorithm, but its accuracy is less than the others. It might fail to meet the accuracy requirement.

In beyond 5G, The THz frequency range might be utilized, which will come with an ultra-massive antenna system (i.e., more than 256). The estimation accuracy of all algorithms will be improved; however, complexity will rise. If the use case requires RMSE of 0.1^o, FFT can achieve that when using 256 elements. Using FFT for AoA gives three advantages. First, FFT's complexity is not increasing with using ultra massive antenna systems for AoA estimation, as explained in **section 5.4.3.1**. Second, it is a robust

algorithm regarding the immunity against the multipath signals and SNR level. The third advantage of using FFT is that this algorithm does not require any prior knowledge about the number of sources.

Stating the advantages of using the FFT algorithm does not mean that it can be the solution in all scenarios. For example, in the sub-6 band, that number of antenna elements does not exist. Especially in highway and rural areas, therefore for such scenarios, a fast-accurate algorithm should be used. CASCADE LOS is the best choice according to the simulation results and as explained in the following:

- It has the best accuracy among the others in the highly correlated signals scenario, as shown in **Figure 5.10**.
- Except for FFT and ESPRIT, it has the shortest running time when antenna elements are less than 150, as shown in **Figure 5.11**.

Table 5.8: Comparison between AoA algorithms

	BF	MVDR	MUSIC	ESPRIT	FFT	CASCADE	CAS-LOS
Accuracy	good	V.good	V.good	Moderate	Bad	V.good	V.good
Resolution	Bad	Moderate	V.good	V.good	Bad	V.good	No Data
# of snapshots	Moderate	Bad	Moderate	Bad	good	Moderate	Moderate
SNR	good	Moderate	Moderate	Bad	V.good	Moderate	Moderate
Correlation	good	Bad	Bad	Bad	V.good	Bad	V.good
Complexity	Moderate	Moderate	Bad	V.good	V.good	Moderate	good

Bad | Moderate | good | V.good | No Data

Table 5.8 gives an overall comparison of the AoA algorithms. The results in this section showed that MUSIC, MVDR, CASCADE, and CASCADE LOS are the best in accuracy in moderate and high SNR. The accuracy is the minimum error that a particular algorithm offers. The focus was, as mentioned previously, on estimating the LOS correctly.

Regarding the resolution, it was shown in **Figure 5.6** that BF, and FFT have the worst resolution among the other algorithms, while MVDR has a moderate level of resolution. MUSIC and its variants, as well as ESPRIT, have the best resolution. The resolution is significant in case it is required to estimate more than one multipath signal. The number of snapshots is a critical parameter for most algorithms; however, MVDR and ESPRIT are the most affected by reducing the number of snapshots. FFT is evaluated as good in snapshots because the original FFT works with only one snapshot. Few snapshots can be used for FFT to average the spatial spectrum of those **N** snapshots.

A low signal-to-noise ratio reduces the accuracy of all algorithms; however, during the simulation, it was shown that some algorithms are robust against the changes in SNR, such as FFT. Also, it was noticed that ESPRIT demands high SNR to reach the same degree of accuracy as the other algorithms such as MUSIC. The impact of SNR can be seen in **Figure 5.8**, **Figure 5.9**, and **Figure 5.4.**

It was explained that the correlation between the incoming signals leads to a deterioration in the algorithm's performance. The results in **Figure 5.10** proved that some methods performed very well when the number of incoming signals increased. FFT and CASCADE LOS are the best, and then the BF comes to a lesser degree.

Regarding the complexity, it was shown in **Figure 5.11** and **Figure 5.12**, the lowest complexity is offered by ESPRIT and FFT, then the CASCADE LOS comes.

Table 5.8 can be considered as a guideline for selecting the algorithm with respect to a certain application. Also, it gives an intuition of what should be taken into account when designing a new algorithm for estimating AoA.

6. CONCLUSION

The main objective of the thesis was to investigate the different methods for Angle of Arrival (AoA) estimation that can be used for enhancing the positioning in the 5G system and beyond. Also, to investigate how the new technologies offered by the 5G systems can boost the estimation of AoA, which was included for the first time in 3GPP standards.

The thesis started by covering the capability of the 5G system for positioning by illustrating the different measurements methods standardized according to 3GPP. Furthermore, the enabler technologies in 5G systems have been covered and linked to the positioning problem. For example, massive antenna systems and mm-waves are among the most powerful technologies that boost the positioning in 5G to meet the requirement of the different use cases. It was also explained in **section 2** the new signals for positioning in 5G by highlighting the features of those signals. The network architecture that responsible for handling the positioning signal was explained in **section 2** as well**.**

As the foundation of estimate AoA, the fundamentals of array signal processing and smart antenna systems were presented in **section 3**. Later in the mentioned section, the mathematical model of estimating the AoA by extracting the phase information from signals impinging on the array element was illustrated. **Section 3** provided the necessary background information before moving on to Section 4's discussion of AoA estimate techniques.

Section 4 includes a review of the literature, the state of the art in estimating AoA, and a detailed comparison of traditional AoA estimation algorithms, highlighting the differences in the mathematical model and the limitations of those algorithms in mobile communication, in order to determine whether those algorithms can meet the requirements of 5G positioning.

In the section, a CASCADE technique was proposed to solve the major issues of the MUSIC algorithm, which is the most common AoA estimate algorithm. Although MUSIC is a high-resolution technique, it has a high level of complexity that makes it inappropriate for many applications. Furthermore, like with many AoA algorithms, the correlated signals significantly impact the MUSIC algorithm. The proposed CASCADE method is based on narrowing the MUSIC algorithm's searching region while generating the spatial spectrum. This was accomplished by utilizing the FFT method, as the fast AoA algorithm, to determine the coarse range of AoAs and then to pass that range to the MUSIC algorithm in the second stage. That combination offers a remarkable reduction in time consumption compared to the traditional MUSIC algorithm. In terms of the influence of correlated signals (multipath signals), CASCADE LOS was employed to concentrate only on detecting the LOS and eliminate the correlated signal effect, as shown previously in **Figure 5.10.**

The results of a simulation of six algorithms from **section 4** implemented in MATLAB to evaluate their performance in a realistic setting are presented in **section 5**. Those algorithms are Bartlet beamformer, MVDR, MUSIC, ESPRIT, FFT, and the proposed CASCADE algorithm. The SRS signal generated according to 3GPP standards was used as the input signal for those algorithms. The multipath signals were represented as LOS copies with different attenuation and delay.

The following are the major findings from the thesis research about what was stated in each section:

- The new generation of mobile communication 5G NR offers new methods for positioning measurement and many enabler technologies that can enhance the

localization's accuracy—for instance, mm-waves, massive MIMO, and large bandwidth.

- The sounding reference signal (SRS) is the main positioning signal in the uplink direction. It provides some benefits of using it instead of other reference signals. The most important feature is for the same root zadoff sequence; zero is the cross-correlation between various cyclically shifted sequences, which is the most significant characteristic. This enables the base station to segregate users and therefore minimize interference.
- According to 3GPP, the use case requirements for positioning include the accuracy and complexity represented by latency. The accuracy varies between a few meters and a few millimeters. While the time needed to report the information ranges between a few seconds and a few milliseconds, as shown in **Figure 2.8.**
- Uniform Linear Array can estimate either azimuth or elevation angles. Planner array antenna can be used for estimating both azimuth and elevation.
- The massive array antenna has a remarkable impact on improving the accuracy in estimating the Angle of Arrival. It was observed that the more antenna elements deployed, the more accurate the AoA algorithm becomes.
- Certain factors should be taken into account while developing or choosing an AoA algorithm for 5G positioning. These factors include the algorithm's degree of accuracy, the effect of SNR on the algorithm, the impact of the number of snapshots, the resolution, immunity to correlated signals, and complexity.
- There is a tradeoff between improving the accuracy of estimation and increasing the complexity of the system. The AoA algorithm's consumption time, for example, will rise if more antennas are used. On the other hand, the FFT method is the only one in this thesis whose complexity does not increase as the number of antennas increases.
- The proposed CASCADE LOS algorithm provides the best performance among all algorithms when using less than 64 antenna elements. The evaluation considers the degree of accuracy, complexity, and immunity against the correlated signals.
- In an ultra-massive array system (e.g., 256,512,1024), an FFT algorithm will suffice.

The thesis assessed the performance of many AoA algorithms in the context of the ULA system. ULA, on the other hand, provides for the estimation of either azimuth or elevation angles. Therefore, it is recommended as future work to repeat those algorithms in a planner array system to estimate both azimuth and elevation angles. Additionally, the measurement of AoA should be included in a positioning algorithm, such as a triangulation technique or joint positioning, to demonstrate how the estimate error in the AoA methodology impacts the overall positioning accuracy.

Although line of sight is not always available, the positioning algorithm should properly localize the UE even when there is no line of sight (NLOS). This needs further study to determine how to use the multipath signal for positioning. That issue will also be addressed in future work.

Another future work topic is an investigation on using Machine Learning techniques to measure AoA. This can be done using SRS for channel estimation by using one of the supervising learning such as Multilayer perceptron (MLP), Convolutional Neural Network (CCN), or Recurrent neural network (RNN).

ANNEX I

Generating 5G Uplink waveform:

MATLAB 2021a offers a direct way to generate 5G waveforms (Downlink and Uplink) by using the 5G toolbox, which comes with built-in functions as well as the applications that serve as the function.

The Uplink signal was generated using MATLAB 2021a 5G application as shown below, and then it was exported as an m-file:

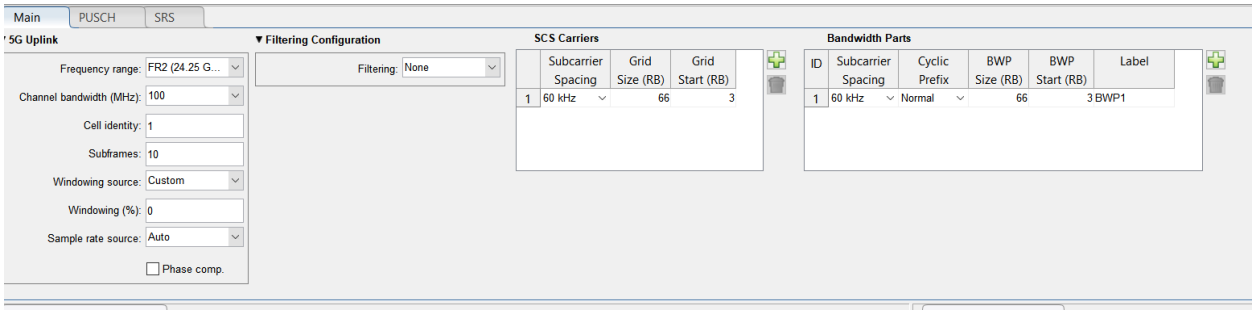

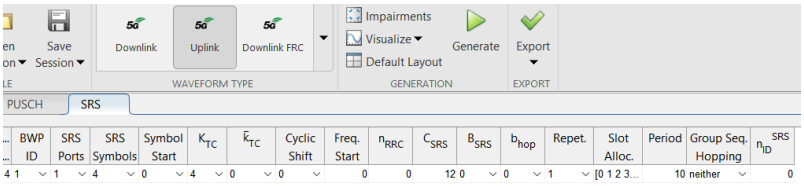

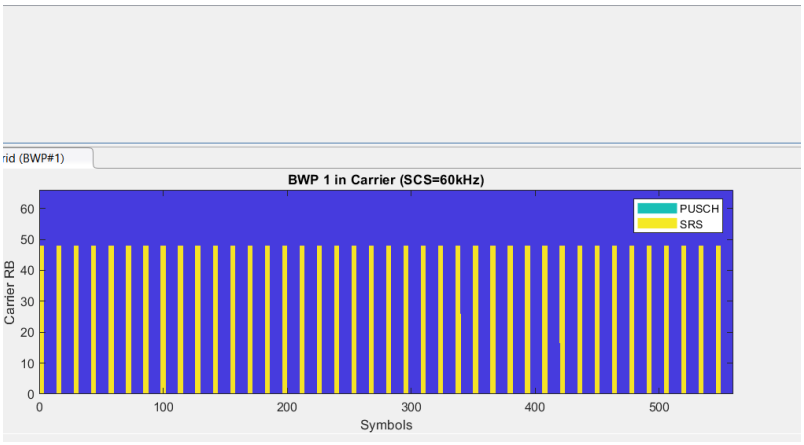

LIST OF SYMBOLS

TDoA	Time Difference of Arrival
v_p	Propagation velocity
RTT	Round Trip Time
T_{ri}	Received signal time
τ_t	Clock bias of the base station
$T_{t,s}$	The transmission time by the transmitter
$T_{r,acl}$	The acknowledgment time
c	Speed of light
f_c	Carrier frequency
λ	Wavelength
ULA	Uniform Linear Array
Δ	The distance between adjacent elements in ULA
X	Received data by the array antenna
$a(\theta)$	Steering vector
θ	Angle of Arrival
β	Phase shift constant
M	Number of Antenna elements
N	Number of snapshots
SNR	Signal to noise ratio
K	Number of multipath signals
S	Transmitted signal
W	Weight Vector for the beamformer
A	Steering matrix
y	The output of the beamformer
τ_m	Time delay
B	Bandwidth
x_m	Received signal at mth antenna element
T	Sampling Time
n	AWGN
R_{XX}	Covariance matrix
σ^2	Noise variance
$I_{M\times M}$	Identity Matrix

$\mathbb{E}$	Statistical expectation
$(\,)^H$	Conjugate transpose (Hermitian)
$\hat{R}$	Estimated Covariance matrix
U_s	Signal subspace
U_n	Noise subspace
σ_s	Singular value
Φ	Diagonal matrix of the phase shift introduced by the second sub-array in ESPRIT
Ψ	rotating subspace
N_{FFT}	FFT length,
S_{CAS}	The minimized searching length in the CASCADE method.
T_{End}	The recorded time after executing the last line of the algorithm,
r	is the number of trials.
T_{Start}	The recorded time at the beginning of the algorithm, and
$\hat{\theta}_k$	is the estimated Angle,
θ_{true}	The actual Angle.

ABBREVIATIONS - ACRONYMS

AoA	Angle of Arrival
DoA	Direction of Arrival
5G	Fifth Generation
MIMO	Multiple Input Multiple Output
mm-waves	Millimeter waves
FR1	Frequency Range 1 in 5G
FR2	Frequency Range 2 in 5G
UE	User Equipment
RAN	Radio Access Network
NGRAN	New Generation RAN
LMF	Location management function
gNB	New Generation Node B
AMF	Access and Mobility management function
LPP	LTE positioning protocol
RCC	Radio resource control protocol
RB	Resource Block
SRS	Sounding Reference Signal
PRS	Positioning Reference Signal
NR	New Radio
SL	Switched lobe
PA	Phased Array
AA	Adaptive Array
AD	Analog to Digital Convertor
SS	Spatial Spectrum
ULA	Uniform Linear Array
SVD	Singular Value Decomposition
EVD	Egien Value Decomposition
BF	Bartlett Beamformer
MVDR	Minimum Variance Distortion less
MUSIC	Multiple Signal Classification
ESPRIT	Estimation of Signal Parameters via Rotational Invariance Technique
FFT	Fast Fourier Transform

LS	Least-squares estimation method
TLS	Total Least Squares estimation method
RMSE	Root Mean Square Error
ELTM	Elapsed Time Metric

REFERENCES

[1] S. Spinsante and C. Stallo, “Hybridized-GNSS Approaches to Train Positioning: Challenges and Open Issues on Uncertainty,” *Sensors*, vol. 20, no. 7, 2020, doi: 10.3390/s20071885.

[2] 3GPP, “3GPP TS 22.261 V18.0.0 - Service requirements for the 5G system,”2020.[Online].Available: https://portal.3gpp.org/desktopmodules/Specifications/SpecificationDetails.aspx?specificationId=3107

[3] 3GPP, “3GPP Technical Report (TR) 22.804 V16.3.0 - Service requirements for the 5G system.”

[4] T. S. Rappaport *et al.*, “Wireless Communications and Applications Above 100 GHz: Opportunities and Challenges for 6G and Beyond,” *IEEE Access*, vol. 7, pp. 78729–78757, 2019, doi: 10.1109/ACCESS.2019.2921522.

[5] A. Bourdoux *et al.*, “6G White Paper on Localization and Sensing.” 2020.

[6] J. A. del Peral-Rosado, R. Raulefs, J. A. López-Salcedo, and G. Seco-Granados, “Survey of Cellular Mobile Radio Localization Methods: From 1G to 5G,” *IEEE Communications Surveys Tutorials*, vol. 20, no. 2, pp. 1124–1148, 2018, doi: 10.1109/COMST.2017.2785181.

[7] S. Dwivedi *et al.*, “Positioning in 5G networks.” 2021.

[8] K. Witrisal *et al.*, “Whitepaper on New Localization Methods for 5G Wireless Systems and the Internet-of-Things.” 2018.

[9] TSGR, “TS 138 305 - V16.1.0 - 5G; NG Radio Access Network (NG-RAN); Stage 2 functional specification of User Equipment (UE) positioning in NG-RAN (3GPP TS 38.305 version 16.1.0 Release 16),” 2020, Accessed: Sep. 04, 2021. [Online]. Available: https://portal.etsi.org/TB/ETSIDeliverableStatus.aspx

[10] A. Gosh, R. Keating, D. Michalopoulos, M. Saily, and B. Vejlgaar, “The Evolution of 5G New Radio Positioning Technologies - Nokia Bell Labs,” 2021. https://www.bell-labs.com/institute/white-papers/evolution-5g-new-radio-positioning-technologies (accessed Sep. 04, 2021).

[11] A. Cardalda Garc´ıa, “Hybrid Localization Algorithm for LTE.” University of Oviedo, 2015.

[12] A. García, S. Maier, and A. Phillips, *Location-Based Services in Cellular Networks: from GSM to 5G NR*. Artech, 2020.

[13] P. Wu, S. Su, Z. Zuo, X. Guo, B. Sun, and X. Wen, “Time Difference of Arrival (TDoA) Localization Combining Weighted Least Squares and Firefly Algorithm,” *Sensors*, vol. 19, no. 11, 2019, doi: 10.3390/s19112554.

[14] C. Mobile *et al.*, “5G Positioning Open API Industry White Paper,” 2021. [Online]. Available: https://www-file.huawei.com/-/media/corporate/pdf/news/5g-positioning-open-api-industry-white-paper-en.pdf?la=en

[15] ETSI 3GPP 5G, “5G; NR; User Equipment (UE) Radio Transmission and Reception; Part 1: Range 1 Standalone (3GPP TS 38.101-1 version 16.4.0 Release 16),” 2018. [Online]. Available: https://portal.etsi.org/TB/ETSIDeliverableStatus.aspx

[16] T. S. Rappaport, G. R. MacCartney, M. K. Samimi, and S. Sun, “Wideband Millimeter-Wave Propagation Measurements and Channel Models for Future Wireless Communication System Design,” *IEEE Transactions on Communications*, vol. 63, no. 9, pp. 3029–3056, 2015, doi: 10.1109/TCOMM.2015.2434384.

[17] S. Sun, T. S. Rappaport, R. W. Heath, A. Nix, and S. Rangan, “Mimo for millimeter-wave wireless communications: beamforming, spatial multiplexing, or both?,” *IEEE Communications Magazine*, vol. 52, no. 12, pp. 110–121, 2014, doi: 10.1109/MCOM.2014.6979962.

[18] I. Akyildiz and J. Jornet, “Realizing Ultra-Massive MIMO (1024×1024) communication in the (0.06–10) Terahertz band,” *Nano Communication Networks*, vol. 8, 2016, doi: 10.1016/j.nancom.2016.02.001.

[19] C. Masterson, “Massive MIMO and Beamforming : The Signal Processing Behind the 5 G Buzzwords,” 2017.

[20] Jukka Westhues, “5G networks will be dense and unforgiving: Why dynamic, automated inventory is critical (Reader Forum),” 2020. https://www.rcrwireless.com/20200812/opinion/readerforum/5g-networks-will-be-dense-and-unforgiving-reader-forum

[21] J. Li, “LOS probability modeling for 5G indoor scenario,” in *2016 International Symposium on Antennas and Propagation (ISAP)*, 2016, pp. 204–205.

[22] 3GPP, “3GPP TR 38.913 V14.3.0 (2017-06) 3rd Generation Partnership Project; Technical Specification Group Radio Access Network; Study on Scenarios and Requirements for Next Generation Access Technologies; (Release 14).”

[23] ERICSSON, “5g-positioning--what-you-need-to-know.” https://www.ericsson.com/en/blog/2020/12/5g-positioning--what-you-need-to-know

[24] Mathworks, “NR Positioning Reference Signal.” https://www.mathworks.com/help/5g/ug/5g-new-radio-prs.html

[25] 3GPP, “3rd Generation Partnership Project; Technical Specification Group Radio Access Network; NR; Physical channels and modulation (Release 15),” 2018. [Online]. Available: http://www.3gpp.org

[26] B. Sun, B. Tan, W. Wang, and E. S. Lohan, “A Comparative Study of 3D UE Positioning in 5G New Radio with a Single Station,” *Sensors*, vol. 21, no. 4, 2021, doi: 10.3390/s21041178.

[27] E. Dahlman, S. Parkvall, and J. Sköld, “Chapter 1 - Introduction,” in *4G LTE-Advanced Pro and The Road to 5G (Third Edition)*, Third Edit., E. Dahlman, S. Parkvall, and J. Sköld, Eds. Academic Press, 2016, pp. 1–5. doi: https://doi.org/10.1016/B978-0-12-804575-6.00001-7.

[28]: Subhash Kumawa, “5G NR Reference signals | DMRS,PT-RS,CSI-RS,SRS.” https://www.rfwireless-world.com/5G/5G-NR-Reference-Signals-DMRS-vs-PTRS-vs-CSI-RS-vs-SRS.html

[29] E. Holzman, “Introduction to Direction-of-Arrival Estimation (Chen, Z.; 2010) [Reviews and Abstracts],” *IEEE Antennas and Propagation Magazine*, vol. 53, no. 1, pp. 110–111, 2011, doi: 10.1109/MAP.2011.5773580.

[30] T. N. Rao and V. S. Rao, “Evaluation of MUSIC algorithm for a smart antenna system for mobile communications,” in *2012 International Conference on Devices, Circuits and Systems (ICDCS)*, 2012, pp. 67–71. doi: 10.1109/ICDCSyst.2012.6188676.

[31] S. Haykin, J. P. Reilly, V. Kezys, and E. Vertatschitsch, “Some aspects of array signal processing,” in *IEE Proceedings F-Radar and Signal Processing*, 1992, vol. 139, no. 1, pp. 1–26.

[32] C. A. Balanis, *Antenna theory: analysis and design*. John wiley \& sons, 2015.

[33] R. Schmidt, “Multiple emitter location and signal parameter estimation,” *IEEE Transactions on Antennas and Propagation*, vol. 34, no. 3, pp. 276–280, 1986, doi: 10.1109/TAP.1986.1143830.

[34] E. Gentilho, P. R. Scalassara, and T. Abrão, “Direction-of-Arrival Estimation Methods: A Performance-Complexity Tradeoff Perspective,” *Journal of Signal Processing Systems*, vol. 92, no. 2, pp. 239–256, 2020.

[35] B. Friedlander, “Wireless Direction-Finding Fundamentals,” 2009, pp. 1–51. doi: 10.1016/B978-0-12-374524-8.00001-5.

[36] J. Capon, “High-resolution frequency-wavenumber spectrum analysis,” *Proceedings of the IEEE*, vol. 57, no. 8, pp. 1408–1418, 1969, doi: 10.1109/PROC.1969.7278.

[37] Y. Jiang, P. Stoica, Z. Wang, and J. Li, “Capon beamforming in the presence of steering vector errors and coherent signals,” in *11th Annual Workshop on Adaptive Sensor Array Processing (ASAP 2003)*, 2003, pp. 11–13.

[38] J. Zhuang, H. Xiong, W. Wang, and X. Cai, “FFT-based adaptive 2-D DOA estimation for arbitrary array structures,” in *2017 22nd International Conference on Digital Signal Processing (DSP)*, 2017, pp. 1–5. doi: 10.1109/ICDSP.2017.8096099.

[39] F. Wen, Q. Wan, R. Fan, and H. Wei, “Improved MUSIC Algorithm for Multiple Noncoherent Subarrays,” *IEEE Signal Processing Letters*, vol. 21, no. 5, pp. 527–530, 2014, doi: 10.1109/LSP.2014.2308271.

[40] R. Roy and T. Kailath, “ESPRIT-estimation of signal parameters via rotational invariance techniques,” *IEEE Transactions on Acoustics, Speech, and Signal Processing*, vol. 37, no. 7, pp. 984–995, 1989, doi: 10.1109/29.32276.

[41] J. Foutz, A. Spanias, and M. K. Banavar, “Narrowband direction of arrival estimation for antenna arrays,” *Synthesis Lectures on Antennas*, vol. 3, no. 1, pp. 1–76, 2008.

[42] N. P. Waweru, D. B. O. Konditi, and P. K. Langat, “Performance analysis of MUSIC, root-MUSIC and ESPRIT DOA estimation algorithm,” *International Journal of Electronics and Communication Engineering*, vol. 8, no. 1, pp. 209–216, 2014.

[43] Z. Aliyazicioglu, H. K. Hwang, M. Grice, and A. Yakovlev, “Sensitivity Analysis for Direction of Arrival Estimation using a Root-MUSIC Algorithm.,” *Engineering Letters*, vol. 16, no. 3, 2008.

[44] H. Krim and M. Viberg, “Two decades of array signal processing research: the parametric approach,” *IEEE Signal Processing Magazine*, vol. 13, no. 4, pp. 67–94, 1996, doi: 10.1109/79.526899.

[45] I. Moazzen and P. Agathoklis, “A Multistage Space–Time Equalizer for Blind Source Separation,” *Circuits, Systems, and Signal Processing*, vol. 35, 2015, doi: 10.1007/s00034-015-0042-4.

[46] T. Kim and S. Hwang, “Cascade AOA Estimation Algorithm Based on Flexible Massive Antenna Array,” *Sensors*, vol. 20, no. 23, 2020, doi: 10.3390/s20236797.

[47] N. Bnilam, E. Tanghe, J. Steckel, W. Joseph, and M. Weyn, “ANGLE: ANGular Location Estimation Algorithms,” *IEEE Access*, vol. 8, pp. 14620–14629, 2020, doi: 10.1109/ACCESS.2020.2966519.

[48] N. Maletic, V. Sark, J. Gutiérrez, and E. Grass, “Device Localization Using mmWave Ranging with Sub-6-Assisted Angle of Arrival Estimation,” in *2018 IEEE International Symposium on Broadband Multimedia Systems and Broadcasting (BMSB)*, 2018, pp. 1–6. doi: 10.1109/BMSB.2018.8436861.

[49] N. BniLam, J. Steckel, and M. Weyn, “Synchronization of Multiple Independent Subarray Antennas: An Application for Angle of Arrival Estimation,” *IEEE Transactions on Antennas and Propagation*, vol. 67, no. 2, pp. 1223–1232, 2019, doi: 10.1109/TAP.2018.2880014.

[50] C. Qin, J. A. Zhang, X. Huang, K. Wu, and Y. J. Guo, “Fast Angle-of-Arrival Estimation via Virtual Subarrays in Analog Antenna Array,” *IEEE Transactions on Wireless Communications*, vol. 19, no. 10, pp. 6425–6439, 2020, doi: 10.1109/TWC.2020.3003397.

[51] J. Li, D. Jiang, and X. Zhang, “DOA Estimation Based on Combined Unitary ESPRIT for Coprime MIMO Radar,” *IEEE Communications Letters*, vol. 21, no. 1, pp. 96–99, 2017, doi: 10.1109/LCOMM.2016.2618789.

[52] R. Pöhlmann, S. A. Almasri, S. Zhang, T. Jost, A. Dammann, and P. A. Hoeher, “On the Potential of Multi-Mode Antennas for Direction-of-Arrival Estimation,” *IEEE Transactions on Antennas and Propagation*, vol. 67, no. 5, pp. 3374–3386, 2019, doi: 10.1109/TAP.2019.2899010.

[53] Y. D. Zhang, S. Qin, and M. G. Amin, “Doa estimation exploiting coprime arrays with sparse sensor spacing,” in *2014 IEEE International Conference on Acoustics, Speech and Signal Processing (ICASSP)*, 2014, pp. 2267–2271. doi: 10.1109/ICASSP.2014.6854003.

[54] W. Du and R. L. Kirlin, “Improved spatial smoothing techniques for DOA estimation of coherent signals,” *IEEE Transactions on Signal Processing*, vol. 39, no. 5, pp. 1208–1210, 1991, doi: 10.1109/78.80975.

[55] P. Gerstoft, A. Xenaki, C. F. Mecklenbräuker, and E. Zochmann, “Multiple snapshot compressive beamforming,” in *2015 49th Asilomar Conference on Signals, Systems and Computers*, 2015, pp. 1774–1778. doi: 10.1109/ACSSC.2015.7421456.

[56] 3GPP, “3GPP. 5G; NR; Physical Channels and Modulation. Technical Specification (TS) 38.211, 3rd Generation Partnership Project (3GPP), V15.3.0.,” 2018. [Online]. Available: https://www.etsi.org/deliver/etsi_ts/138200_138299/138211/15.03.00_60/ts_138211v150300p.pdf

[57] “What are Mean Squared Error and Root Mean Squared Error?,” 2018. https://www.vernier.com/til/1014

[58] R. Zhang, K. Xu, Y. Quan, S. Zhu, and M. Xing, “Signal Subspace Reconstruction for DOA Detection Using Quantum-Behaved Particle Swarm Optimization,” *Remote Sensing*, vol. 13, no. 13, 2021, doi: 10.3390/rs13132560.

[59] R. Hunger, *Floating Point Operations in Matrix-Vector Calculus*, vol. Version 1. Munich University of Technology, Inst. for Circuit Theory and Signal~…, 2007.